

TM ST 0701

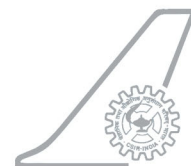
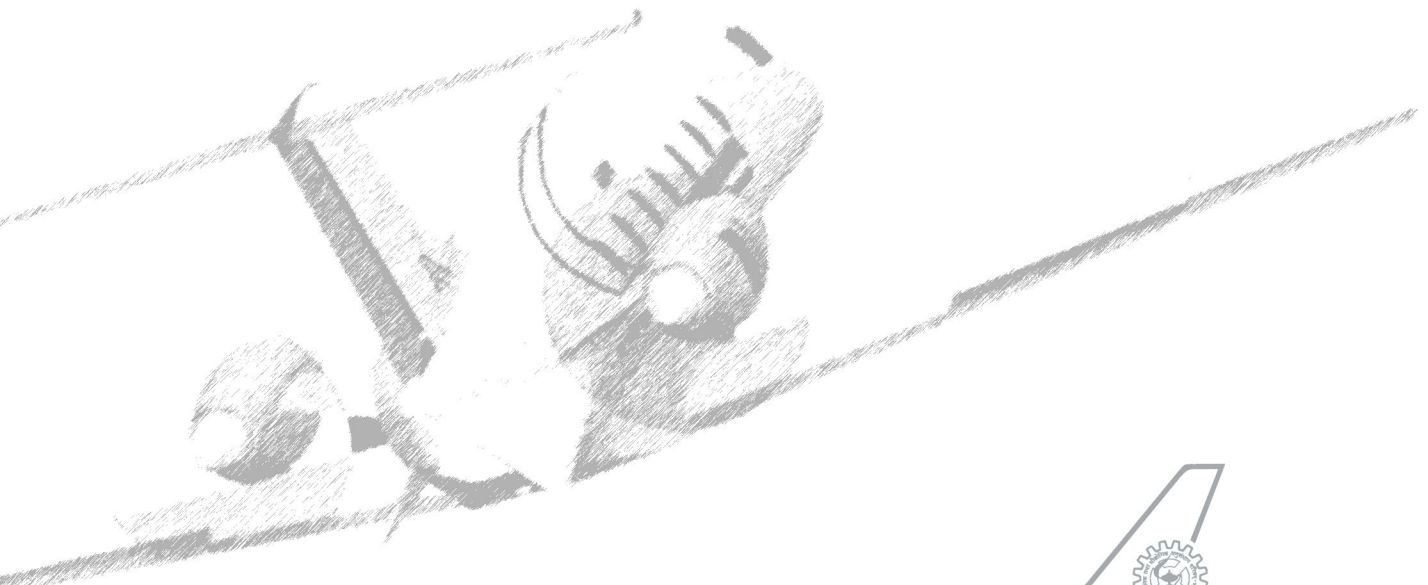
Restricted

Finite Element Studies on Supersonic Panel Flutter under High Thermal Environment with Arbitrary Flow Direction

SOMENATH MUKHERJEE, M MANJUPRASAD, AVINASH R,
DEEPA SAKRAVARTHINI S

Project Co-ordinator : Dr. S SRIDHARA MURTHY
Structures Division

Technical Memorandum ST 0701
October 2007



National Aerospace Laboratories

Bangalore 560 017, India

ABSTRACT

Panels of re-entry vehicles are subjected to a wide range of flow conditions during ascent and re-entry phases. The flow can vary from subsonic continuum flow to hypersonic rarefied flow with wide ranging dynamic pressure and associated aerodynamic heating. One of the main design considerations is the assurance of safety against panel flutter under the flow conditions characterized by harsh thermal environment. The objectives of this work are to understand the physical principles behind panel flutter under supersonic flow and to make an estimate of the lowering of the critical dynamic pressure (flutter boundary) of the panels due to thermal distributions.

Analytical and Finite element formulation have been developed for supersonic flutter analysis of rectangular panels subjected various thermal profiles. The piston theory is used for aerodynamic pressure computations. Panels with simply supported edges (with and without in-plane edge constraints) have been studied.

The results obtained by NASTRAN for flow along panel edges are in good agreement with those obtained using the analytical method and the in-house FEM code. From the analysis of the results for various flow directions it has been observed that the flow along the longer sides of the panels is most critical. For simply supported panels with no in-plane edge constraints a thermal gradient can cause a drastic fall in the flutter boundary due to in-plane thermal stresses that effectively reduce structural stiffness. In-plane edge constraints to thermal expansion further lower the flutter boundary.

The present study will be useful for the purpose of panel design in re-entry launch vehicles and supersonic fighter aircrafts.

CONTENTS

	Page No.
Abstract	
Chapter 1 Analytical and Finite Element Formulation of Supersonic Panel Flutter under Thermal Environment with Arbitrary Flow Direction	1-11
1.1 Introduction	1
1.2 Literature review	1
1.3 Analytical Formulation for Supersonic Panel Flutter	2
1.4 Basic equations	3
1.5 Solution of the differential equation	4
1.6 Finite Element Formulation for Supersonic Panel Flutter	5
1.6.1 Strain Energy	6
1.6.2 Work done due to in-plane stress resultant	6
1.6.3 Expression for Aerodynamic loads	7
1.6.4 Kinetic Energy	7
1.6.5 Equation of Motion	7
1.7 Supersonic Panel Flutter Analysis with NASATRAN	8
1.7.1 Aerodynamic theory	9
1.7.2 P-K Method for Flutter solution	9
1.7.3 Supersonic flutter analysis of panels	10
1.7.4 Supersonic panel flutter analysis with Thermal loads	10
Chapter-2 Numerical results for Panels of given configuration without Thermal effect	12-17
2.1 Introduction	12
2.2 Free Vibration Analysis of a Panel of various Aspect ratios (without thermal effects)	12
2.3 Modal Coalescence in Panel Flutter and Critical Dynamic Pressure (without thermal effects) for flow along one of the edges (say side a , $\theta=0$)	14
2.4 Influence of flow angularity on critical flow parameters	16
2.5 Chapter Summary and Observations	17
Chapter 3 Flutter results for Panels of given configuration with Thermal effect	18-37
3.1 Numerical Studies for Supersonic Panel Flutter with Thermal Effect	18
3.1.1 Thermal buckling analysis of rectangular panels of aspect ratios 1, 2 and 7.2 (specimens A, B and C), simply supported on all edges with in-plane edge constraints.	18

3.2	Effect of Parabolic Temperature Distribution (without in-plane edge constraints) over simply supported rectangular panels of aspect ratio 1, 2 and 7.2 (specimens A, B and C)	19
3.2.1	Thermal stress distribution due to parabolic temperature distribution	19
3.2.2	<i>Effect of Parabolic Temperature Distribution on flutter boundary (without in-plane edge constraints) over simply supported rectangular panels with airflow along x-direction (edge a, $\theta = 0$)</i>	20
3.2.3	<i>Effect of flow direction on the flutter boundary</i>	24
3.3	Effect of uniform Edge Loads due to edge constraints on thermal expansion on the flutter boundary of rectangular panels.	31
3.3.1	<i>Effect of Uniform Edge Loading due to edge constraint on thermal expansion with flow along x-direction (edge a, $\theta = 0$)</i>	31
3.3.2	<i>Effect of flow direction on the flutter boundary of panels with various thermal profiles and in-plane edge constraints</i>	33
3.4	Variation of Critical boundary (Mach number) with altitude	35
3.5	Effect on mass loading due to Thermal Protection System (TPS) mass	36
3.6	Chapter Summary and Observations	37
Chapter 4	Conclusion	38-39
	References	40
	APPENDIX A	42
	APPENDIX B	49

Chapter 1

ANALYTICAL AND FINITE ELEMENT FORMULATION OF SUPERSONIC PANEL FLUTTER UNDER THERMAL ENVIRONMENT WITH ARBITRARY FLOW DIRECTION

1.1 Introduction

The panels that form the skin of re-entry launch vehicles are subjected to harsh thermal environment, especially in the supersonic and hypersonic regimes of flight. Usually a Thermal Protection System (TPS layer) is provided to protect the metallic skin from getting overheated. Despite this TPS, some temperature rise is anticipated in the metallic skin. The objective of present work is to investigate, using analytical, in-house finite element methods and finite element package NASTRAN, the effects of a parabolic thermal profile on the flutter boundary of isotropic, simply supported rectangular panels. Piston theory has been used for calculating aerodynamic forces under supersonic airflow condition. The PK-method is adopted for flutter analysis in NASTRAN.

1.2. Literature review

Excellent treatises on the classical theory of aeroelasticity have been presented by Fung [1], Bisplinghoff and Ashley [2]. The physics and computational aspects of various kinds of static and dynamic aeroelastic problems have been highlighted. The earliest study of flutter seems to have been made by Lanchester [3], Bairstow and Fage [4] in 1916 in connection with the anti symmetrical (fuselage torsion-elevator torsion) flutter of a Handleg Page Bomber. Up to 1934, only a few cases of flutter were recorded. In those days only airplane wings showed flutter. Aileron mass unbalance and low torsional stiffness of the wing were responsible for most of these accidents.

The aeroelastic instability of aircraft skin panels has been the subject of a number of theoretical investigations. During the second world war of 1939-1945, Germany launched a number of V2 missiles. Many of these missiles failed during flight, the cause of which was later recognized as supersonic flutter of the missile fins [5]. In his analysis of supersonic flutter, Ashley developed a simple mathematical formula, based on a theory called the "Piston Theory" to estimate the aerodynamic loads for supersonic flow. In the early part of world war, most of the flutter cases were due to insufficient aileron mass balance and most tail-surface flutter cases were due to control surface tabs. Towards the latter part of world war, airplane speed increased towards the transonic range, and supersonic missiles appeared.

Early experimental and theoretical studies of the flutter behavior of buckled plates were carried out by Fung [6]. The primary concern was with the prediction of stability boundaries, although Fung did derive modal equations of motion for finite amplitude motions of the plate. Herman and Sidney [7] have compared experimental results with the theoretical predictions of panel flutter, and have concluded that the linearized, quasi-steady aerodynamic theory is valid only beyond Mach 1.3.

Stability boundaries for buckled two-dimensional plate were calculated by Hedgepeth [8] using an approach similar to Fung. Hedgepeth's application of the two-dimensional static aerodynamic approximation to the panel flutter problem. It greatly simplified the analytical complexities and resulted in a differential equation that can be solved exactly for finite panels. It has shown that a system of uniform stresses can greatly reduce the flutter speed of an unbuckled panel. During 1950's, several experimental investigations were conducted to

verify the existence of panel flutter and to determine some of the effect of such parameters as panel length-width ratio, thickness, and differential pressure.

The effect of buckling on flutter boundaries of three-dimensional plates was investigated by Fralich [9]. He used Von Karman large deflection plate equations and Ackeret's expression for the aerodynamic pressure. The equations were transformed into pair of nonlinear ordinary differential equation by Galerkin's method, using the first two modes of a simply supported plate as coordinate function. A stability analysis is carried out for each buckling load by linearizing these equations about the buckled configuration, and computing the eigenvalues in the usual manner.

In many problems of panel flutter the most obvious methods of analysis have been to apply the Galerkin's method using the governing equations of the problem. The applicability of the Galerkin's method to the supersonic membrane flutter problem has been studied by Ellen [10] and found to give good agreement with exact solutions.

Using piston theory and analytical methods, Harry and Walter [11] had reported the results of their investigation for the flutter behaviour of simply supported, thermally stressed square panel subjected to supersonic airflow along one edge of the panel. Erickson [12] has also reported the results of panel flutter investigation for orthotropic panels.

Using C^1 type Rectangular Plate Element for finite element method, Zienkiewicz O. C [13] has presented shape function for geometry and displacements. Timoshenko S.P. [14] has presented the elastic equation for plate bending

Sander et al [15] have employed the finite element method for supersonic flutter analysis using a new conforming quadrilateral (CQ) element.

Thermal Structures for aerospace application by Earl A. Thornton [16] gives an authoritative source on design and analysis of aerospace structures in thermal environment.

The analytical formulation and non-dimensional results for supersonic panel flutter under thermal environment with flow in arbitrary direction has been presented by Mukherjee et al [17, 18]

The combined documentation (NASTRAN) [19] provides the required information for aero-modeling which is required for flutter analysis

1.3. Analytical Formulation for Supersonic Panel Flutter

The panel configuration and its discretization are shown in Fig 1.1 The rectangular panel of length ' a ', width ' b ', and uniform thickness ' h ' is simply supported on all edges with no in-plane constraints. It is subjected to a supersonic airflow at Mach number ' M ' along the direction making an angle ' θ ' with the edge ' a ' of the panel.

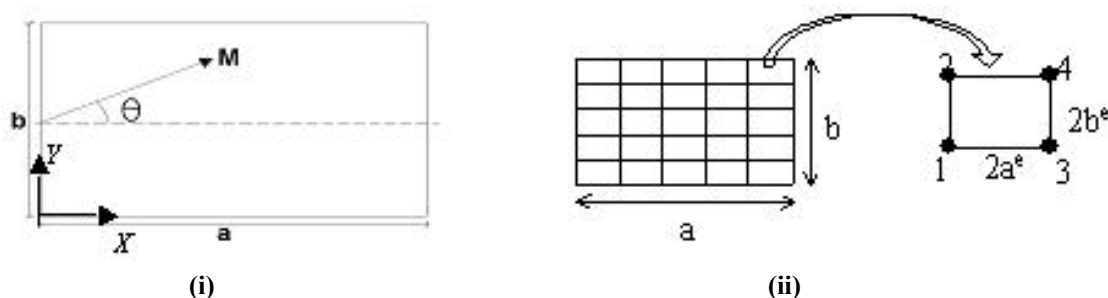


Fig 1.1 (i) Panel under flow along the direction of angle ' θ ' with the edge ' a ' and (ii) The FEM discretization of the rectangular panel into rectangular elements each of size $2a^e \times 2b^e$.

The panel is subjected to a parabolic temperature distribution in the middle plane as in Fig 1.2, with temperature difference of ΔT_1 between the center and the edges. The parabolic temperature distribution over the panel is given mathematically by the function

$$T(x, y) = 16\Delta T_1 \left(\frac{x}{a}\right) \left(1 - \frac{x}{a}\right) \left(\frac{y}{b}\right) \left(1 - \frac{y}{b}\right) \quad (1.1)$$

where the rise in temperature at the panel center with respect to the edges is given by $\Delta T_1 = T_{center} - T_{edges}$.

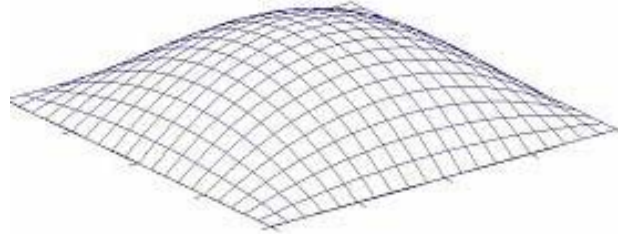


Fig 1.2 Parabolic temperature distribution over the rectangular panel.

1.4. Basic equations

The equation of motion of the panel under a loading per unit area is given as

$$D\nabla^4 w + N_x \frac{\partial^2 w}{\partial x^2} + 2N_{xy} \frac{\partial^2 w}{\partial x \partial y} + N_y \frac{\partial^2 w}{\partial y^2} + \rho_{mat} h \frac{\partial^2 w}{\partial t^2} = p \quad (1.2)$$

Here w is the transverse displacement (due to dynamic pressure) which is a function of x , y and time t , $D = \frac{Eh^3}{12(1-\mu^2)}$ is flexural rigidity of the panel, E is the Young's modulus, μ is the

Poisson's ratio and h is the thickness of the plate. The net *in-plane* axial stress resultants (assumed positive for compression) per unit width along x - and y -directions of the panel are denoted by N_x and N_y , respectively, which is the sum of those induced by uniform, normal forces at the boundary (N_{x0} and N_{y0}) and those resulting from the parabolic temperature distribution (N_{xT} and N_{yT}) while the shear loading is denoted by N_{xyT} . The mass per unit area of the panel is $\rho_{mat}h$ where ρ_{mat} is the mass density of the panel material. The unsteady aerodynamic pressure load p is obtained by use of linearized, quasi-steady, two-dimensional aerodynamics (Piston theory), originally proposed by Ashley. According to this theory, the unsteady aerodynamic pressure over the panel is given by

$$p = -\frac{2q}{\sqrt{M^2 - 1}} \left(\frac{\partial w}{\partial x} \cos \theta + \frac{\partial w}{\partial y} \sin \theta \right) \quad (1.3)$$

Here q is the dynamic pressure ($q = \rho_{air} V^2/2$), V is the flow speed and M is the supersonic Mach number.

The thermally induced in-plane stress resultants, from the parabolic temperature profile alone, vanish at the boundaries that do not offer any constraints to in-plane thermal expansion. These are determined in terms of stress function $\phi = \phi(x, y)$, given by [11],

$$\phi = C \alpha E h a^2 \Delta T_1 \left(\frac{x}{a}\right)^2 \left(\frac{x}{a} - 1\right)^2 \left(\frac{y}{b}\right)^2 \left(\frac{y}{b} - 1\right)^2 \quad (1.4a)$$

The condition that the panel be free from thermally induced in-plane normal and shear stresses on the boundaries (due to parabolic temperature alone) requires that the stress function satisfy the following boundary conditions.

$$\begin{aligned} \phi(0, y) = \phi(a, y) = \phi(x, 0) = \phi(x, b) = 0 \\ \frac{\partial \phi}{\partial x}(0, y) = \frac{\partial \phi}{\partial x}(a, y) = \frac{\partial \phi}{\partial y}(x, 0) = \frac{\partial \phi}{\partial y}(x, b) = 0 \end{aligned} \quad (1.4b)$$

For compatibility of in-plane strains, the stress function must satisfy the following partial differential equation.

$$\nabla^4 \phi = \alpha E h \nabla^2 T \quad (1.5)$$

where α is the coefficient of thermal expansion. Applying Galerkin's technique to equation (1.5), the expression for the constant C can be obtained as.

$$C = -\frac{6(1+\beta^2)}{1+\left(\frac{4}{7}\right)\beta^2+\beta^4}, \quad \beta = \frac{a}{b} \quad (1.6)$$

Thus the in-plane stress resultants from the parabolic thermal profile are given as

$$\begin{aligned} N_{xT} &= \frac{\partial^2 \phi}{\partial y^2} = C \alpha E h a^2 \Delta T_1 \left(\frac{x}{a}\right)^2 \left(\frac{x}{a}-1\right)^2 \left(\frac{12y^2}{b^4} - \frac{12y}{b^3} + \frac{2}{b^2}\right) \\ N_{yT} &= \frac{\partial^2 \phi}{\partial x^2} = C \alpha E h a^2 \Delta T_1 \left(\frac{12x^2}{a^4} - \frac{12x}{a^3} + \frac{2}{a^2}\right) \left(\frac{y}{b}\right)^2 \left(\frac{y}{b}-1\right)^2 \\ N_{xyT} &= -\frac{\partial^2 \phi}{\partial x \partial y} = -C \alpha E h a^2 \Delta T_1 \left(\frac{4x^3}{a^4} - \frac{6x^2}{a^3} + \frac{2x}{a^2}\right) \left(\frac{4y^3}{b^4} - \frac{6y^2}{b^3} + \frac{2y}{b^2}\right) \end{aligned} \quad (1.7)$$

The net in-plane force intensity terms in equation (1.2) is written as

$$\begin{aligned} N_x &= N_{x0} + N_{xT} \\ N_y &= N_{y0} + N_{yT} \\ N_{xy} &= N_{xyT} \end{aligned} \quad (1.8a)$$

Uniform edge loads from in-plane edge constraints to thermal expansion, develops due to the difference of *mean* temperature T_{mean} of the panel from the reference temperature $T_{reference}$, at which the edge loading vanishes. One can approximate these edge loads (per unit edge length) from edge constraints to thermal expansion as

$$N_{x0} = N_{y0} = \frac{E}{(1-\mu)} \alpha (\Delta T_2) h \quad (1.8b)$$

Here the effective panel temperature ΔT_2 for edge loads is defined as

$$\Delta T_2 = T_{mean} - T_{reference}$$

The mean panel temperature T_{mean} of the panel with uniform edge temperature T_{edge} and with the parabolic thermal profile $T(x,y)$ (as in equation (1.1)) is given by

$$T_{mean} = T_{edge} + \frac{\int_0^a \int_0^b T(x,y) dy dx}{\int_0^a \int_0^b dy dx} = T_{edge} + \frac{4}{9} \Delta T_1$$

Thus one can finally express the effective temperature as

$$\Delta T_2 = T_{edge} + \frac{4}{9} \Delta T_1 - T_{reference} \quad (1.8c)$$

1.5. Solution of the differential equation

For panels with all edges having simply supported conditions to transverse deflection, the solution of equation (1.2) can be represented as follows

$$w(x,y,t) = \sum_{m=1}^{\infty} \sum_{n=1}^{\infty} a_{mn} \sin \frac{m\pi x}{a} \sin \frac{n\pi y}{b} e^{i\omega t} \quad (1.9)$$

Here ω is the circular frequency and t is the time. This function satisfies the following kinematic and the kinetic boundaries conditions of the simply supported edges of the panel.

$$w(0, y, t) = w(a, y, t) = w(x, 0, t) = w(x, b, t) = 0$$

$$\frac{\partial^2 w}{\partial x^2}(0, y, t) = \frac{\partial^2 w}{\partial x^2}(a, y, t) = \frac{\partial^2 w}{\partial y^2}(x, 0, t) = \frac{\partial^2 w}{\partial y^2}(x, b, t) = 0 \quad (1.10)$$

After substituting equations (1.3), (1.8) and (1.9) into equation (1.2) and then applying Galerkin's procedure, one obtains the following set of equations for the amplitude coefficients a_{mn} .

$$\left\{ \left[r^2 + \left(\frac{a}{b} \right)^2 s^2 \right]^2 - R_{x_0} r^2 - R_{y_0} \left(\frac{a}{b} \right)^2 s^2 \right\} a_{rs}$$

$$- k^2 a_{rs} + \lambda L_{rs} + \left\{ \frac{C}{5\pi^2} \left(\frac{a}{b} \right)^2 \left[\left(\frac{r}{s} \right)^2 + \left(\frac{s}{r} \right)^2 \right] a_{rs} + \frac{8C}{\pi^2} \left(\frac{a}{b} \right)^2 K_{rs} \right\} \psi = 0 \quad (1.11)$$

where $\psi = \frac{\alpha E h a^2 \Delta T_1}{\pi^2 D}$, $k^2 = \frac{\rho_{mat} h a^4 \omega^2}{\pi^4 D}$, $\lambda = \frac{2 q a^3}{D \sqrt{M^2 - 1}}$, $R_{x_0} = \frac{N_{x_0} a^2}{\pi^2 D}$, $R_{y_0} = \frac{N_{y_0} a^2}{\pi^2 D}$

$$K_{rs} = M_{rs} + P_{rs} - 4 Q_{rs} - (1/40) \left[(r/s)^2 + (s/r)^2 \right] a_{rs}$$

The parameter k^2 is the non-dimensional frequency. The parameter λ is the non-dimensional form of the dynamic pressure, The non-dimensional parameters R_{x_0} and R_{y_0} accounts for any additional *in-plane* loading along the edges of the panel, either from mechanical sources or from *constraints* to *in-plane thermal expansion* at the edges and the terms L_{rs} , M_{rs} , P_{rs} and Q_{rs} are presented in [17,18]. Here $r=1,2\dots M_x$ and $s=1,2\dots M_y$ where M_x and M_y are the number of modes superposed along x and y directions of the panel respectively in equation (1.9).

Since the problem is of determining the stability of a given form of solution, it is advantageous to associate the eigenvalue with the frequency parameter k^2 . For flow speeds beyond a critical flow velocity V_{cr} , the system becomes *dynamically unstable* when k^2 becomes *complex*. The imaginary part of $\sqrt{-k^2}$ represents the non-dimensional frequency. The real part of $\sqrt{-k^2}$, when positive, indicates that the system motion diverges in amplitude in an oscillating fashion. Thus from equation (1.11) it is possible to determine the critical values of the non-dimensional dynamic pressure λ_{cr} at which the oscillatory motion of the panel changes from a periodic to an unstable diverging amplitude type. This critical condition is associated with modal coalescence of two or more modes. Using modal superposition method eigenvalues are calculated, and the lowest value of λ_{cr} for where two of the eigenvalues coalesce is sought. Details of the analysis has been presented in an earlier reports [17,18].

1.6. Finite element formulation for supersonic panel flutter

For the present work a Quad4 C^1 continuity element is selected. At each node in an element there are three displacement components, *viz.* the transverse displacement w and the slopes about x and y -axes. The unsteady nodal displacement vector at node i is expressed in the following equation using the cubic polynomial shape function matrix $[N^b]$ and the time dependent nodal displacement vector $\{d^e\}$.

$$\{d_i\} = \{w_i \quad \theta_{xi} \quad \theta_{yi}\}^T = \left\{ w_i \quad - \left(\frac{\partial w}{\partial y} \right)_i \quad \left(\frac{\partial w}{\partial x} \right)_i \right\}^T \quad (1.12)$$

$$w = [N^b] \{d^e\} = [N_1^b \quad N_2^b \quad N_3^b \quad N_4^b] \{d_i\}, \quad \{d_i\} = \{d_1 \quad d_2 \quad d_3 \quad d_4\}^T \quad (1.13)$$

where the $[N_i^b]$ are the C^l shape function matrices for any node in terms natural, local co-ordinates

$$\xi = \frac{(x - x_c)}{a^e}, \quad \eta = \frac{(y - y_c)}{b^e} \quad (1.14)$$

where (x_c, y_c) are the global co-ordinates of the center of the element. For the C^l displacement interpolation in equation (1.13), the shape function matrix for node i ($i=1,2,3,4$), is given by

$$[N_i^b] = \frac{1}{8} \begin{bmatrix} (\xi_o + 1)(\eta_o + 1)(2 + \xi_o + \eta_o - \xi^2 - \eta^2) \\ a^e \xi_i (\xi_o + 1)^2 (\xi_o - 1)(\eta_o + 1) \\ b^e \eta_i (\xi_o + 1)(\eta_o + 1)^2 (\eta_o - 1) \end{bmatrix}^T \quad \xi_o = \xi \xi_i, \eta_o = \eta \eta_i \quad (1.15)$$

1.6.1. Strain Energy

The strain component vector $\{\varepsilon\}$ as given in [13] can be expressed in terms of strain-displacement matrix $[B]$ in terms of normalized co-ordinates,

$$\{\varepsilon\} = \left[-\frac{\partial^2 w}{\partial x^2} \quad -\frac{\partial^2 w}{\partial y^2} \quad 2\frac{\partial^2 w}{\partial x \partial y} \right]^T = [B] \{d^e\} = [B_1 \quad B_2 \quad B_3 \quad B_4] \{d^e\} \quad (1.16)$$

Here the component $[B_i]$ of the strain-displacement matrix at node i is given as

$$[B_i] = \left[-\frac{1}{a^{e^2}} \frac{\partial^2 N_i^b}{\partial \xi^2} \quad -\frac{1}{b^{e^2}} \frac{\partial^2 N_i^b}{\partial \eta^2} \quad \frac{1}{a^e b^e} 2 \frac{\partial^2 N_i^b}{\partial \xi \partial \eta} \right]^T \quad (1.17)$$

The strain energy expression U can be expressed in terms element bending stiffness matrix $[K^e]$ as

$$U = \frac{1}{2} \int \{\varepsilon\}^T [D] \{\varepsilon\} dx dy = \frac{1}{2} \{d^e\}^T [K^e] \{d^e\} \quad (1.18)$$

Here $[D]$ is the plate flexural rigidity matrix, and $[K^e]$ is the element bending stiffness matrix given by

$$[D] = D \begin{bmatrix} 1 & \mu & 0 \\ \mu & 1 & 0 \\ 0 & 0 & (1 - \mu)/2 \end{bmatrix} \quad (1.19)$$

$$[K^e] = a^e \times b^e \int_{-1}^1 \int_{-1}^1 [B]^T [D] [B] d\xi \quad (1.20)$$

The full form of the element bending stiffness matrix $[K^e]$ is presented in the Appendix A equation (A.3).

1.6.2. Work done due to in-plane stress resultant

The panel is subjected in-plane thermal stresses in its mid-plane. The work done due to the net in-plane stresses as given in [15] is expressed as

$$W_s = \frac{1}{2} \iint \left(\left[\frac{\partial w}{\partial x} \quad \frac{\partial w}{\partial y} \right] [N_m] \left[\frac{\partial w}{\partial x} \quad \frac{\partial w}{\partial y} \right]^T \right) dx dy \quad (1.21)$$

Here $[N_m]$ is net mid-plane stress intensity matrix, represented as

$$[N_m] = \begin{bmatrix} N_x & N_{xy} \\ N_{xy} & N_y \end{bmatrix} \quad (1.22)$$

where N_x , N_y , and N_{xy} , are the net in-plane stress resultant intensity (force per unit length) as presented in equation (1.8a). Using the transformation rule for element geometry (equation (1.14)), one can express $[N_m]$ in terms of the local normalized coordinates ξ and η . Thus from equation (1.21), we finally have the expression for the work done by in-plane forces as

$$W_s = \frac{1}{2} \{d^e\}^T [K_s^e] \{d^e\} \quad (1.23)$$

where $[K_s^e]$ is the element stiffness matrices associated with net in-plane stress resultants. These are expressed as

$$[K_s^e] = a^e b^e \int_{-1}^1 \int_{-1}^1 \left(\begin{bmatrix} \frac{1}{a^e} \frac{\partial N^b}{\partial \xi} \\ \frac{1}{b^e} \frac{\partial N^b}{\partial \eta} \end{bmatrix}^T [N_m] \begin{bmatrix} \frac{1}{a^e} \frac{\partial N^b}{\partial \xi} \\ \frac{1}{b^e} \frac{\partial N^b}{\partial \eta} \end{bmatrix} d\xi d\eta \right) \quad (1.24)$$

The matrices $[K_s^e]$ is evaluated for every element using four point Gaussian quadrature rule of integration along each of the two direction ξ and η (see Appendix A for equation form and Gauss points).

1.6.3. Expression for Aerodynamic loads

Substituting the expression for p into the virtual work done by aerodynamic forces W_a as given in [15] and expressing w in terms of normalized co-ordinates, we obtain the expression for virtual work done by aerodynamic forces as

$$W_a = \int p w dx dy = -\{d^e\}^T \left([K_{qx}^e] \cos \theta + [K_{qy}^e] \sin \theta \right) \{d^e\} = -\{d^e\}^T [K_q^e] \{d^e\} \quad (1.25)$$

where

$$[K_{qx}^e] = \int_{-1}^1 \int_{-1}^1 \frac{2q}{\sqrt{M^2 - 1}} \left(\begin{bmatrix} \frac{1}{a^e} \frac{\partial N^b}{\partial \xi} \\ \frac{1}{b^e} \frac{\partial N^b}{\partial \eta} \end{bmatrix}^T [N^b] \right) a^e b^e d\xi d\eta, \quad [K_{qy}^e] = \int_{-1}^1 \int_{-1}^1 \frac{2q}{\sqrt{M^2 - 1}} \left(\begin{bmatrix} \frac{1}{a^e} \frac{\partial N^b}{\partial \xi} \\ \frac{1}{b^e} \frac{\partial N^b}{\partial \eta} \end{bmatrix}^T [N^b] \right) a^e b^e d\xi d\eta \quad (1.26)$$

The full form of the element aerodynamic load matrix $[K_{qx}^e]$ and $[K_{qy}^e]$ are presented in the Appendix A equation (A.4) and (A.5) respectively.

1.6.4. Kinetic Energy

The kinetic energy expression T that defines the consistent mass matrix $[M^e]$ is expressed as follows

$$T = \frac{1}{2} \int \rho_{mat} \left[\frac{dw}{dt} \right]^2 dv = \frac{1}{2} \rho_{mat} h \int \dot{w}^T \dot{w} dx dy = \frac{1}{2} \{d^e\}^T [M^e] \{d^e\} \quad (1.27)$$

Here $[M^e]$ is the element consistent mass matrix expressed in terms of normalized co-ordinates and is given by

$$[M^e] = h \rho_{mat} \int \int [N^b]^T [N^b] a^e b^e d\xi d\eta \quad (1.28)$$

The full form of the element consistent mass matrix $[M^e]$ is presented in the Appendix A equation (A.6)

1.6.5. Equation of Motion

The element assembly process implies the following summations

$$U^g = \sum_e U^e, \quad W_s^g = \sum_e W_s^e, \quad W_a^g = \sum_e W_a^e, \quad T^g = \sum_e T^e \quad (1.29)$$

The stiffness matrix $[K^e]$, initial stress matrix $[K_s^e]$, aerodynamic load matrix $[K_q^e]$ and consistent mass matrix $[M^e]$ for every element are generated and assembled in proper order to obtain the global stiffness matrix $[K^g]$, initial stress matrix $[K_s^g]$, aerodynamic load matrix $[K_q^g]$ and mass matrix $[M^g]$. The total strain energy U_T^g of the assembly is the sum of global strain energy U^g and the global work done due to the in-plane membrane stresses W_s^g ,

$$U_T^g = U^g + W_s^g = \frac{1}{2} \{d^g\}^T ([K^g] + [K_s^g]) \{d^g\} \quad (1.30)$$

The generalized aerodynamic forces Q_i is given by

$$Q_i = \frac{\partial W_a}{\partial \{d^g\}} = -[K_q^g] \{d^g\} \quad (1.31)$$

The Lagrange's equation expressed in terms of strain energy, kinetic energy and generalized aerodynamic forces as.

$$\frac{d}{dt} \left(\frac{\partial T^g}{\partial \dot{d}_i^g} \right) + \frac{\partial U_T^g}{\partial d_i^g} = Q_i \quad (1.32)$$

This gives the equation of motion as

$$([K^g] + [K_s^g] + [K_q^g]) \{d^g\} + [M^g] \{\ddot{d}^g\} = 0 \quad (1.33)$$

A modal superposition method will now be used to solve equation (1.33) using a modal superposition of any selected n modes (encapsulated into the modal matrix $[\phi] = [\{\phi_1\}, \{\phi_2\}, \{\phi_3\}, \dots, \{\phi_n\}]$). The dynamic displacement and accelerations vectors of the plate are given as

$$\{d^g\} = [\phi] \{v\} e^{\gamma t}, \quad \{\ddot{d}^g\} = \gamma^2 [\phi] \{v\} e^{\gamma t} \quad (1.34)$$

The parameter γ is complex where $\gamma = \gamma_r + j\gamma_i$. Here γ_i represents the circular frequency ω , and γ_r represents the amplitude increase ($\gamma_r > 0$) or amplitude decrease ($\gamma_r < 0$) with time. Substituting equation (1.34) in equation (1.33) and pre-multiplying by $[\phi]^T$, we get

$$([K_{gen}^g] + [K_{sgen}^g] + [K_{qgen}^g] + \gamma^2 [M_{gen}^g]) \{v\} = \{0\}$$

For non-trivial solutions, we now have the following eigenvalue problem with $-\gamma^2$ as the eigenvalue,

$$|[K_{Tgen}^g] - (-\gamma^2) [M_{gen}^g]| = 0 \quad (1.35)$$

where $[K_{Tgen}^g] = [K_{gen}^g] + [K_{sgen}^g] + [K_{qgen}^g]$. As stated earlier, the generalised stiffness matrix $[K_{gen}^g]$, the generalised in-plane stress intensity matrix $[K_{sgen}^g]$ and the mass matrix $[M_{gen}^g]$ are the diagonal matrices due to the orthogonality of the natural modes. The aerodynamic matrix $[K_{qgen}^g]$ is an anti-symmetric matrix (indicating the non-conservative nature of the system). Thus $[K_{Tgen}^g]$ is non-symmetric due to the contribution of the aerodynamic matrix $[K_{qgen}^g]$. This implies that some of the eigenvalues $-\gamma^2$ are eventually complex for a certain range of the dynamic pressure q . In general, the eigenvalue can be expressed as a complex number, $\gamma = \gamma_r + j\gamma_i$, ($j = \sqrt{-1}$) where the real part γ_r represents the amplitude increase ($\gamma_r > 0$) or amplitude decrease ($\gamma_r < 0$) with time, and the imaginary part γ_i is the circular frequency ω . The lowest value of dynamic pressure for γ_r is positive ($\gamma_r > 0$) for any mode is the critical dynamic pressure q_{cr} .

1.7. Supersonic Panel Flutter Analysis with NASTRAN

The supersonic flutter analysis module in NASTRAN is also employed here to predict the flutter boundaries under the assumed thermal profiles. The intension of this exercise is to establish the validity of the results simulated by various methods through comparison.

1.7.1. Aerodynamic theory

Piston theory is used for calculating the aerodynamic loads in which the local pressure generated by the body's motion is related to the local normal component of fluid velocity in the same way that these quantities are related at the face of a piston moving in a one-dimensional channel. It is a point function, used to represent aerodynamic pressures on surfaces with small-scale geometric characteristics, (i.e., the pressures are only dependent upon local conditions).

1.7.2. P-K Method for Flutter solution

NASTRAN uses mass and stiffness matrices for dynamic analysis. It pre and post multiplies these matrices by eigenvectors to get generalized mass $[M_{hh}]$ and generalized stiffness $[K_{hh}]$. The user defines the aerodynamic model and the interpolation function between structural and aerodynamic grid points. Based on the aerodynamic theory selected, the aerodynamic influence coefficient Matrix is calculated. It is pre and post multiplied by mode shape to get generalized aerodynamic influence coefficient matrix $[Q_{hh}]$. This generalized aerodynamic coefficient matrix is used in the damping term (for p-k method) of the equation of motion.

The fundamental equation for modal flutter analysis by the p-k method is,

$$[M_{hh} p^2 + (B_{hh} - \frac{1}{4} \rho \bar{c} V Q_{hh}^I / k) p + (K_{hh} + \frac{1}{2} \rho V^2 Q_{hh}^R)] \{u_h\} = 0 \quad (1.36)$$

where the new terms are

Q_{hh}^{RR}, Q_{hh}^I = modal aerodynamic damping matrices as functions of Mach number (M) and reduced frequency (k)

p = complex eigen value = $\omega (\gamma \pm i)$

γ = transient decay rate coefficient (Note: the structural damping coefficient $g = 2\gamma$)

The matrix terms in above equation are all real. Q_{hh}^I and Q_{hh}^R are respectively, the real and imaginary parts of Q_{hh} (m, k). Circular frequency and the reduced frequency are not independent since $k = (\omega c / 2 V)$, and furthermore, that

$$k = (c/2V) \text{Im}(p) \quad (1.37)$$

For the PK-method of solution, equation (1.36) is rewritten in the state-space form with twice the order.

$$[A - pI] \{\bar{u}_h\} = 0 \quad (1.38)$$

where $[A]$ is the real matrix,

$$[A] = \begin{bmatrix} 0 & I \\ -M_{hh}^{-1} [K_{hh} + \frac{1}{2} \rho V^2 Q_{hh}^R] & -M_{hh}^{-1} [B_{hh} - \frac{1}{4} \rho \bar{c} V Q_{hh}^I / k] \end{bmatrix} \quad (1.39)$$

and $\{\bar{u}_h\}$ now includes both modal displacements and velocities. The eigen values of the real matrix $[A]$ are either real or complex conjugate pairs.

In PK-method, the eigenvalues P are first extracted. Convergence for each mode is achieved by feeding the imaginary part of P (frequency ω) as non dimensional frequency k for updating the aerodynamic matrix, till input k equals output k (from P).

If there are multiple densities and mach numbers, the first Mach number and density are printed first, followed by the (optional) second Mach number and second density and finishing with the final Mach number and final density. From the V - g plots (Fig 2.5(b)), the unstable mode can be easily identified as the one that crosses the zero-line of the damping g ($g=2\gamma_r$), indicating that just beyond a certain *critical (flutter)* flow velocity V_{cr} , the damping for that mode becomes positive (from negative), which is an indication of dynamic instability. At the critical velocity, the system is at the flutter boundary.

1.7.3. Supersonic flutter analysis of panels

The panel flutter analysis has been carried out by the PK method. The unsteady air-loads in the supersonic range were calculated using Piston theory for a set of ‘ n ’ normal modes in the generalized coordinates. The CAERO5 bulk data entry specifies the strips width in NSPAN. Each CAERO5 entries specify one PAERO5, which provides the mach numbers and angle of attack values on AEFACT. AERO entry specifies chord length and air density. The MKAERO1 and MKAERO2 bulk data entries allow the selection of parameters for the explicit calculations of the aerodynamic matrices. Flutter analysis is performed based on the parameters specified on the FLUTTER bulk data entry that is selected by the FMETHOD Case Control command. The parameters LMODES or LFREQ and HFREQ can be used to select the number of vibration modes to be used in the flutter analysis and can be varied to determine the accuracy of convergence. The NVALUE field on the FLUTTER entry can be used to limit flutter summary output. These generalized (modal) aerodynamic force coefficient matrices are then interpolated to any additional mach numbers and reduced frequencies required by the flutter analysis. Matrix interpolation is an automatic feature of the program. The first six modes of the plates are considered for flutter analysis. The pertinent output of a flutter solution in NASTRAN comprises of the following: Natural frequencies and Mode shapes, velocity (v) and frequency (f), artificial structural damping and reduced frequency for all modes considered for analysis. Results are analyzed to get the flutter velocity and critical modes leading to flutter. The post processing is carried out using Msc/Patran. From these plots the flutter frequency and critical flutter velocities are calculated for zero damping. The output velocity corresponding to zero damping indicates the speed at which the panel may flutter.

Though NASTRAN requires some initial Mach number as an input data, it produces critical velocities that do not conform to the input Mach number. For agreement with analytical solutions, it is necessary to have an input Mach number in conformity with the critical velocity (and the critical dynamic pressure according to the air density). If the critical velocity determined by NASTRAN does not match input Mach number, then this input Mach number needs to be updated to this critical velocity. This iterative process is continued by updating the input Mach number till the output and input Mach numbers agree. Converged NASTRAN results so obtained can then be compared with those from the analytical solutions. The iterative method for convergence of Mach number is presented in appendix B.

1.7.4. Supersonic panel flutter analysis with Thermal loads

The field of aerothermoelasticity considers the effects of thermally induced stresses on structural stiffness and their aeroelastic interaction. The structural stiffness is reduced at higher temperature. The stiffness matrix has been determined as a function of temperature using the Non-linear Thermal Analysis (Solution Sequence 153). With the temperature-dependent stiffness matrix, restarts can be made in the Aerodynamic Flutter Analysis (Solution Sequence 145) and the variation of flutter speed with temperature is determined.

The uniform temperature distribution over the simply supported panel (with in-plane edge constraints) and parabolic temperature over the panel (with out in-plane edge constraints) has been considered here. The temperature data are entered into TEMP and TEMPD cards. Although no variation of material properties with temperature is considered here, provision is made for variations with temperature by including the MATT1 entry with its associated TABLEMi entries using the same properties at both ends of the tabulated temperature range. The nonlinear parameter entry NLPARM specifies data for the post buckling geometric nonlinear iteration strategy. The KMETHOD is used for controlling the stiffness updates and KSTEP used for specify the number of iterations between stiffness updates. The convergence details and the LOOPID number for the stiffness matrix are saved for the restart. In the restart it is necessary to add the PARAM, NMLOOP to give the value of the LOOPID for the temperature of interest. The Case Control Section for the restart must include some information from the initial run. After the title, subtitle, and echo commands, the initial temperature must be given again. Assign statement has been used to assign the location (with directory) of “MASTER” file, which is used in COLDRUN (SOL.153). The NASTRAN results so obtained can then be compared with those from the analytical solutions.

Chapter 2

NUMERICAL RESULTS FOR PANELS OF GIVEN CONFIGURATION WITHOUT THERMAL EFFECT

2.1. Introduction

The supersonic panel flutter analysis of rectangular panels simply supported on all edges is considered. The panel is subjected to supersonic airflow in arbitrary direction, but restricted to a plane parallel to the plane of the panel. In this analysis the panel is not subjected to any thermal effects. The values of critical dynamic pressure that lead to flutter for panels of various aspect ratios and different flow direction are determined here. Fig 2.1 presents a schematic view of a hinged panel subjected to supersonic airflow, with flow angle θ with respect to the side a .

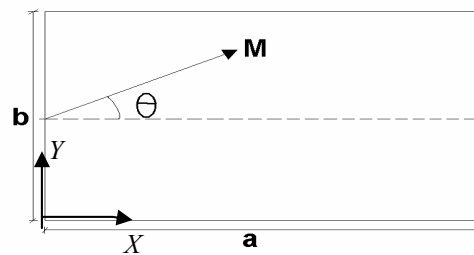


Fig 2.1 Panel under flow along the direction making an angle ' θ ' with the edge ' a ' of the panel.

A numerical study is done by analytical, and in-house finite element code to determine the supersonic flutter boundary of simply supported aluminium panels of aspect ratios 1,2 and 7.2 (see Table 2.1), without thermal effect for different flow angles.

Table 2.1 Dimensions of aluminium panels used as specimens for study of supersonic panel flutter.

Specimen	Length $a(m)$	Width $b(m)$	Thickness $h(m)$	Aspect ratio a/b	Discretisation of panel for FEA	Discretisation of panel for NASTRAN
A	0.25	0.25	0.00232	1.0	100 (10x10)	100 (10x10)
B	1.0	0.5	0.007	2.0	200(20x10)	450(30x15)
C	0.36	0.05	0.0011	7.2	720 (72x10)	720 (20x10)

Young's Elasticity, $E = 70 \times 10^9 \text{ N/m}^2$, Poisson's ratio, $\mu = 0.3$, Coefficient of thermal expansion $\alpha = 2.3 \times 10^{-5} / ^\circ\text{C}$ and Material density $\rho_{mat} = 2764 \text{ kg/m}^3$.

2.2. Free Vibration Analysis of a Panel of various aspect ratios (without thermal effects)

The free vibration analysis is done by analytical, in-house finite element method, and finite element package NASTRAN to determine the natural frequencies of simply supported aluminium panels of aspect ratios 1, 2 and 7.2 (specimens A, B and C respectively). CQUAD4 elements have been used in NASTRAN. The results of the analysis for the first few modes are presented in Tables 2.2-2.4. The discretisation schemes used are presented in Fig 2.2-2.4

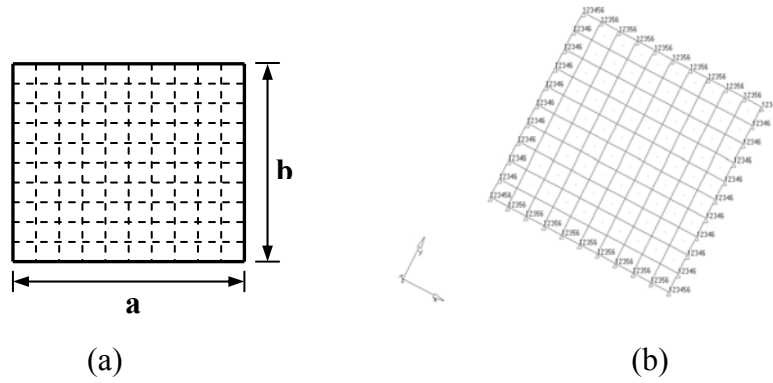


Fig 2.2 Finite element model for square panel (a) in-house FEM, (b) NASTRAN

Table 2.2. Natural frequencies of the square panel (specimen A) with simply supported edges.

Mode (m, n)	Natural Frequency (Hz)		
	Analytical*	in-house FEM Formulation	NASTRAN
(1,1)	177.5933	176.66	175.16
(2,1)	443.9832	440.37	435.14
(3,1)	887.9664	880.43	870.35
(1,2)	443.9832	440.37	435.14
(2,2)	710.3731	696.22	677.95
(3,2)	1154.356	1123.9	1089.5
(1,3)	887.9664	880.43	870.35
(2,3)	1154.356	1123.9	1089.5
(3,3)	1509.543	1498.3	1482.11

*Expression for analytical frequency for any panel of aspect ratio (a/b), vibrating in the (m,n) mode is expressed in equation (2.1)

$$f_{mn} = \frac{\pi}{2} \sqrt{\frac{D}{\rho_{mat} h}} \left(\left(\frac{m}{a} \right)^2 + \left(\frac{n}{b} \right)^2 \right) \quad (2.1)$$

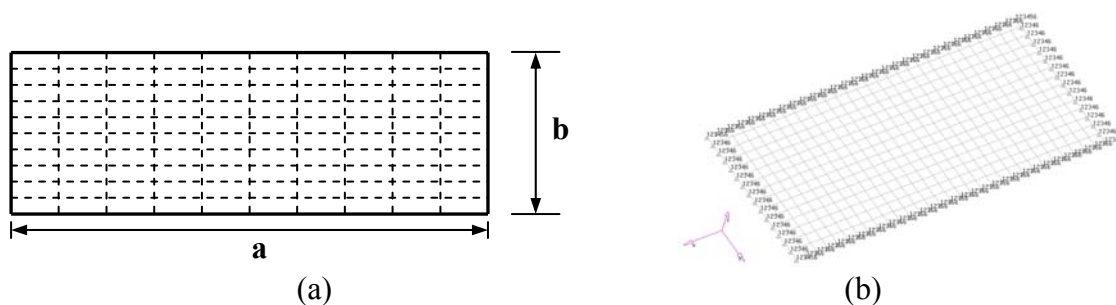


Fig 2.3 Finite element model for panel of aspect ratio (a/b) = 2 (a) in house FEM, (b) NASTRAN

Table 2.3. Natural frequencies of the Rectangular panel of aspect ratio (a/b) =2 (specimen B) with simply supported edges.

Mode (m, n)	Natural Frequency (Hz)			
	Analytical*	in-house FEM Formulation	NASTRAN	
			(20x10)	(30x15)
(1,1)	83.72	83.199	83.22	83.47
(2,1)	133.96	132.24	132.03	133.01
(3,1)	217.68	214.44	213.44	215.55
(1,2)	284.66	282.47	282.52	283.44
(2,2)	334.90	326.84	327.53	331.05
(3,2)	418.62	402.66	402.85	410.41
(1,3)	619.56	614.89	613.98	616.06
(2,3)	669.80	651.24	651.45	660.64
(3,3)	753.53	714.96	715.02	735.04

* as mentioned equation (2.1)

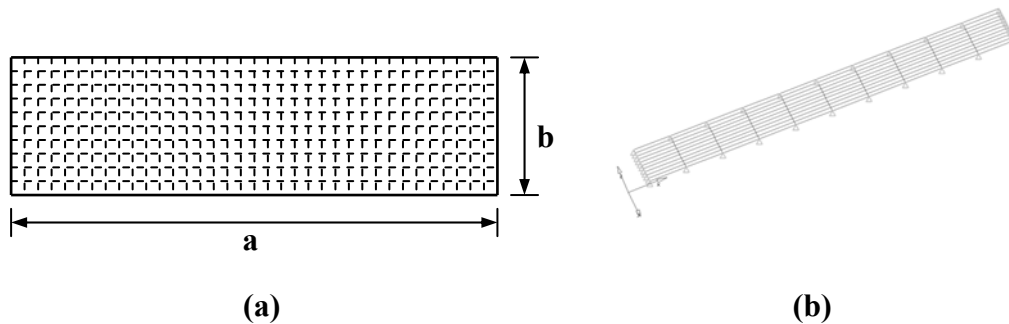


Fig 2.4 Finite element model for panel of aspect ratio (a/b) = 7.2 (a) in house FEM, (b) NASTRAN

Table 2.4 Natural frequencies of the Rectangular panel of aspect ratio (a/b) =7.2 with simply supported edges.

Mode (m, n)	Natural Frequency (Hz)		
	Analytical	in-house FEM Formulation	NASTRAN (72x10)
(1,1)	1073	1072.2	1061.52
(2,1)	1134	1131.0	1090.95
(3,1)	1235	1229.4	1141.41
(1,2)	4230	4228.2	4045.73
(2,2)	4291	4280.8	4127.29
(3,2)	4393	4368.8	4179.79
(1,3)	9493	9492.1	8866.82
(2,3)	9554	9534.6	9159.17
(3,3)	9656	9605.8	9342.30

2.3. Modal Coalescence in Panel Flutter and Critical Dynamic Pressure (without thermal effects) for flow along one of the edges (say side a , $\theta=0$)

Solution of the characteristic equation (1.35) gives the eigenvalue $-\gamma^2$. In particular, as the dynamic pressure q increases from zero, two of the free vibration eigenvalues tend to veer towards each other in such a way that for sufficiently large q (denoted q_{cr}), they coalesce into

a pair of complex-conjugate eigenvalues. One of these complex-conjugate eigenvalues gives a *positive real part* ($\gamma_r > 0$) for the parameter $\gamma = \gamma_r + j\gamma_i$, (where $-\gamma^2$ is the eigenvalue), indicating dynamic instability, characterized by indefinite divergence of amplitude with respect to time in exponential fashion. Upon such coalescence, one of the corresponding mode amplitude would grow by drawing energy from the flow *i.e.* the panel would become unstable. The lowest value of q for which two of the eigenvalues coalesce is the critical value of the dynamic-pressure (q_{cr}), which leads to flutter.

The results for specimen A (square panel) using the in-house FEM code and analytical formulation are presented in Fig 2.5. It is observed that the eigenvalues, for modes (1,1) and (2,1), are purely real and remain so until some higher value of the dynamic pressure, called q_{cr} is reached. At q_{cr} , the two eigenvalues become equal, beyond q_{cr} , and eigenvalues form a complex conjugate pair, indicating the coalescence of the two modes. For an air density of $\rho = 1.225 \text{ kg/m}^3$ the in-house finite element method predicts the occurrence of instability at $V_{cr} = 6202.08 \text{ m/s}$ and $q_{cr} = 23.56 \text{ MN/m}^2$, while the analytical method predicts instability at $V_{cr} = 6287.145 \text{ m/s}$ and $q_{cr} = 24.2 \text{ MN/m}^2$.

For analysis using NASTRAN, free vibration analysis is first performed. This is followed by analysis incorporating aerodynamic matrix as the loading (equation (1.36)), to determine modal frequencies and aerodynamic damping as functions of the flow velocity. These are determined from the eigenvalues. From the V - g plots (Fig 2.5(b)), the unstable mode can be easily identified as the one that crosses the zero-line of the damping ($g = 2\gamma_r$), indicating that just beyond a certain *critical (flutter)* flow velocity V_{cr} , the damping for that mode becomes positive (from negative), which is an indication of dynamic instability. At the critical velocity, the system is at the flutter boundary. The results using NASTRAN are in good agreement with both analytical and in-house FEM formulations. Critical velocity and critical dynamic pressure for specimen A as predicted by NASTRAN are respectively $V_{cr} = 6185.00 \text{ m/s}$ and $q_{cr} = 23.43 \text{ MN/m}^2$. Results obtained by NASTRAN are in good agreement with those obtained using the analytical method and the in-house FEM code.

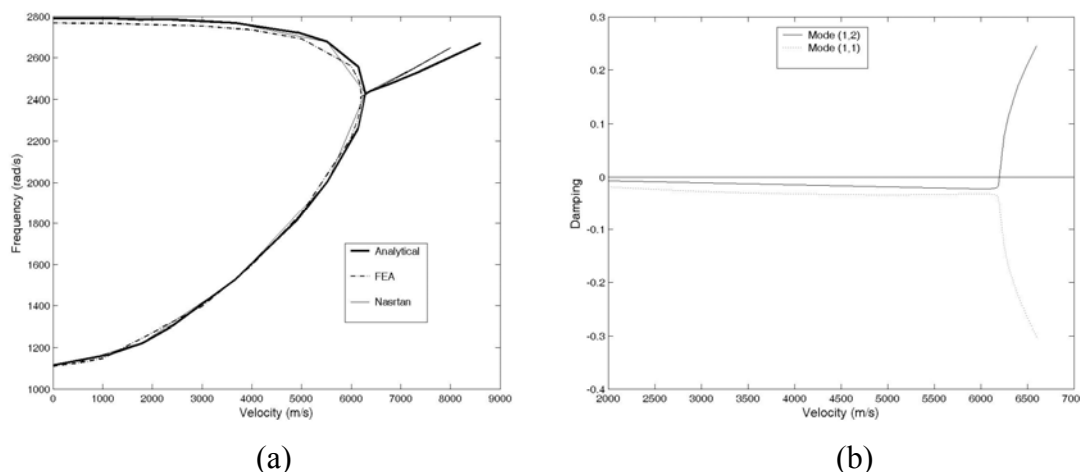


Fig 2.5 (a) Velocity V (m/s) Vs Frequency ω (rad/s) (b) Velocity Vs Damping for a panel of aspect ratio $(a/b) = 1$ (specimen A) and air density $\rho = 1.225 \text{ kg/m}^3$.

Supersonic panel flutter analysis has been done even for simply supported panels of aspect ratio 2 and 7.2, (*i.e.* specimen B with air density of $\rho = 1.225 \text{ kg/m}^3$ and Specimen C with air density of $\rho = 0.715 \text{ kg/m}^3$), both subjected to flow along edge 'a'. The critical parameters (critical dynamic pressure, critical velocity and critical Mach number) of all the specimens A, B and C for supersonic flow along side a are summarized in Table 2.5.

Table 2.5 Comparison of analytical and finite element method results with NASTRAN for panels of aspect ratio 1, 2 and 7.2 (specimens A, B and C respectively) with flow along edge 'a', ($\theta=0$).

Specimen	Dimensions (m) and aspect ratio (a/b)	Non dimensional Critical Dynamic Pressure λ_{cr}	Air density (kg/m^3)	Critical Dynamic Pressure q_{cr} (MPa)	Critical Flow Speed V_{cr} (m/s)	Critical Mach number M_{cr}
A	$a = 0.25$ $b = 0.25$ $h = 0.00232$ (a/b)=1	512	1.225	*24.2 **23.6 #23.43	*6287.145 **6202.08 #6185.00	*18.492 **18.24 #18.19
B	$a = 1.0$ $b = 0.50$ $h = 0.007$ (a/b)=2	1099	1.225	*20.6 **19.2 #20.6	*5796.41 **5593 #5797.50	*17.048 **16.45 #17.05
C	$a = 0.36$ $b = 0.05$ $h = 0.0011$ (a/b)=7.2	9387.5	0.715	*17.8 **16.6 #17.2	*7053.518 **6813.055 #6936.589	*20.74 **20.03 #20.40

Young's Elasticity, $E = 70 \times 10^9 \text{ N/m}^2$, Poisson's ratio, $\mu = 0.3$, Coefficient of thermal expansion $\alpha = 2.3 \times 10^{-5} / ^\circ\text{C}$ and Material density $\rho_{mat} = 2764 \text{ kg/m}^3$.

*Results obtained by analytical formulation; **Results obtained by in-house finite element method formulation; #Results obtained by NASTRAN

2.4. Influence of flow angularity on critical flow parameters

A simply supported rectangular panels with different aspect ratios 1, 2 and 0.5 (specimens A, B and BB which has same thickness as that of specimen B of aspect ratio 2, but the length and width are interchanged to get the correlation between them) subjected to airflow in arbitrary direction is considered. The flow is along the direction making an angle θ with edge 'a' of the panel.

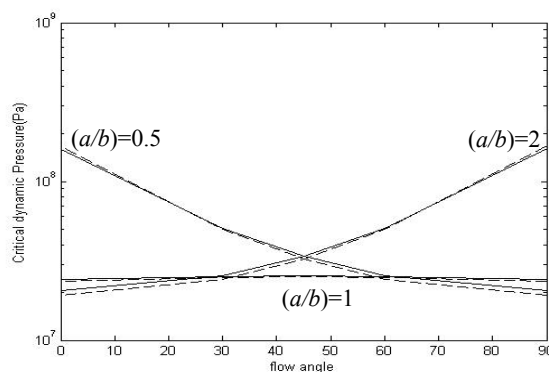


Fig.2.6 Variation of Critical dynamic pressure q_{cr} (in N/m^2), with arbitrary flow direction θ for the specimen panels of various aspect ratios (---FEM, —Analytical). Air density assumed is 1.225 kg/m^3 at sea level. Specimens A, B and BB are of aspect ratios 1, 2 and 0.5 respectively.

The critical dynamic pressures for various flow angles are determined. For a square plate, a symmetric variation of the critical dynamic pressure with flow angle is observed. The critical dynamic pressures q_{cr} at $\theta=0^\circ$ and $\theta=30^\circ$ are same as those at $\theta=90^\circ$ and $\theta=60^\circ$ respectively. The maximum critical dynamic pressure occurs for a flow angle $\theta=45^\circ$, i.e. for a flow equally inclined to both the edges. The results are generated also for panels of aspect ratios 0.5 and aspect ratios 2, with different flow angles. Table 2.6 presents the results

obtained for rectangular simply supported panels of these aspect ratios subjected to various orientations of the flow. These results are given graphically in Fig 2.6. It is clear that for panels with aspect ratios other than 1, the variation of the dynamic pressure is no more symmetric with the flow angle. For aspect ratios below 1, the critical dynamic pressure q_{cr} falls with the flow angle, while for aspect ratios above 1, it increases with the flow angle. *This implies that the flow along the longer side is most critical. i.e. the critical dynamic pressure is lowest for this direction.*

Table 2.6 Influence of flow angularity on flutter boundary of panels with different aspect ratios.

a/b	Analytical Values of Non Dimensional Critical Dynamic Pressure $\lambda_{cr} = \frac{2q_{cr}a^3}{D\sqrt{M_{cr}^2 - 1}}$				
	$\theta = 0^\circ$	$\theta = 30^\circ$	$\theta = 45^\circ$	$\theta = 60^\circ$	$\theta = 90^\circ$
0.5	*383.8 #382	*215 #213	*177 #172	*154 #151	*138 #135
1	*512 #503	*522.08 #516	*525.95 #523	*522.08 #516	*512 #503
2	*1099.9 #1081	*1225 #1206	*1409 #1388	*1719 #1703	*3076.18 #3056

Specimen	Dimensions (m) and aspect ratio (a/b)	Air density (kg/m ³)	Critical Dynamic Pressure q_{cr} (MN/m ²)				
			$\theta=0^\circ$	$\theta=30^\circ$	$\theta=45^\circ$	$\theta=60^\circ$	$\theta=90^\circ$
A	$a = 0.25$ $b = 0.25$ $h = 0.00232$ (a/b)=1	1.225	*24.2 **23.6 #23.4	*25.2 **24.7 #24.6	*25.6 **25.2 #25.3	*25.2 **24.7 #24.6	*24.2 **23.6 #23.4
B	$a = 1.0$ $b = 0.50$ $h = 0.007$ (a/b)=2	1.225	*20.6 **19.2 #19.8	*25.5 **24.1 #24.8	*33.8 **32.4 #32.2	*50.4 **49.8 #49.5	*161 **167 #159
BB	$a = 0.50$ $b = 1.0$ $h = 0.007$ (a/b)=0.5	1.225	*161 **167 #159	*50.4 **49.8 #49.5	*33.8 **32.4 #32.2	*25.5 **24.1 #24.8	*20.6 **19.2 #19.8

*Analytical results (using non-dimensional critical parameter λ_{cr}); **Results obtained by in-house finite element method formulation; # Results presented in Ref [15]

2.5. Chapter Summary and Observations

Supersonic flutter of simply supported rectangular plates of various aspect ratios, subjected to supersonic flows in arbitrary directions in the plane have been studied. No thermal effects are considered here. Results from the analytical formulation, the in-house finite element code and NASTRAN are in good agreement.

The effect of flow angularity on the critical dynamic pressure is investigated here. For a square plate the critical dynamic pressure is symmetric with respect to the flow along $\theta=45^\circ$, at which the maximum critical dynamic pressure occurs. For other aspect ratios, critical dynamic pressure values decrease as the flow gets more and more aligned to the longest direction, with the flow along the longer side being most critical, *i.e.* of the lowest critical dynamic pressure. The high critical Mach numbers predicted by the present analysis based on piston theory aerodynamics only indicate that the specimen panels under the given conditions are extremely stiff, despite the fact that such high Mach numbers do not fall in the regime of piston theory aerodynamics.

Chapter 3

FLUTTER RESULTS FOR PANELS OF GIVEN CONFIGURATION WITH THERMAL EFFECT

3.1. Numerical Studies for Supersonic Panel Flutter with Thermal Effect

A numerical study is done by analytical formulation, in-house finite element method formulation and the FEM software NASTRAN, to determine the supersonic flutter boundary of rectangular panels, with various cases of thermal effects, which are as follows.

1. Parabolic temperature distribution over the panel (without in-plane edge constraints).
2. Uniform temperature distribution over the panel (with edge loads that arise from in-plane constraints at the panel edges).
3. Combination of parabolic and uniform temperature distribution over the panel (with in-plane edge constraints).

The variation of critical parameters (critical dynamic pressure/ critical velocity/ critical Mach number) are investigated for the above cases with different flow directions for some specimen aluminium panels of aspect ratios 1, 2 and 7.2 (see Table 3.1).

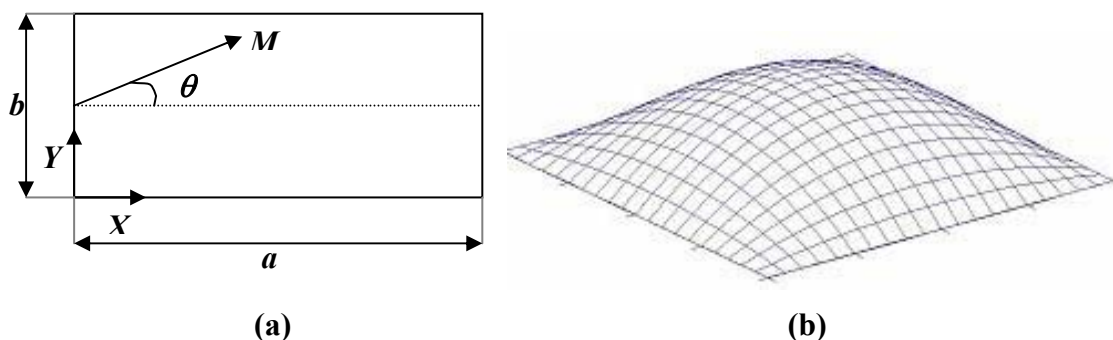


Fig 3.1 (a) Panel under flow along the direction making an angle ‘ θ ’ with the edge ‘ a ’ of the panel, (b) Parabolic Temperature Distribution over the Panel.

Table 3.1 Dimensions of aluminium panels used as specimens for study of supersonic panel flutter.

Specimen	Length $a(m)$	Width $b(m)$	Thickness $h(m)$	Aspect ratio a/b	Discretisation of panel for FEA	Discretisation of panel for NASTRAN
A	0.25	0.25	0.00232	1.0	100 (10x10)	100 (10x10)
B	1.0	0.5	0.007	2.0	200(20x10)	450(30x15)
C*	0.36	0.05	0.0011	7.2	720 (72x10)	720 (20x10)

For aluminium, Young's Elasticity, $E = 70 \times 10^9 \text{ N/m}^2$, Poisson's ratio, $\mu = 0.3$, Coefficient of thermal expansion $\alpha = 2.3 \times 10^{-5} / ^\circ\text{C}$ and material density $\rho_{mat} = 2764 \text{ kg/m}^3$.

* Typical wing panel.

3.1.1. Thermal buckling analysis of rectangular panels of aspect ratios 1, 2 and 7.2 (specimens A, B and C), simply supported on all edges with in-plane edge constraints.

The static buckling temperatures for rectangular panels (simply supported with in-plane edge constraints) of different aspect ratios (specimens A, B and C) have been calculated by analytical, in-house finite element method, and the finite element package NASTRAN. A *constant thermal profile* is used for the analysis. The analytical expression of the buckling temperature for the rectangular panel [16] is given as

$$\Delta T_{buckle} = \frac{(1-\mu)D\pi^2\left(\frac{1}{a^2} + \frac{1}{b^2}\right)}{E\alpha h} \quad (3.1)$$

Buckling analysis is done with stiffness, thermal and inertia matrices, but without the aerodynamic matrices. In the NASTRAN plate model, the edges of the panels are constrained from in-plane thermal expansion. For analytical and in-house FEM code, in-plane edge loads N_{x0} and N_{y0} are computed from the equation (1.8b) for constant temperature rise ΔT_2 (with $\Delta T_1=0$) over the panel. The eigenvalues (and the natural frequencies) computed for various uniform temperature profiles fall with temperature rise, till the buckling temperature is reached at which the natural frequency vanishes. A sample variation of natural frequency with the constant thermal profile for the specimen A ($a/b=1$) is shown in Fig 3.2. Good agreement is observed between analytical and NASTRAN results. Buckling temperature values for the rectangular panels of aspect ratios 1, 2 and 7.2 (specimens A, B and C) obtained by the different methods are presented in Table 3.2.

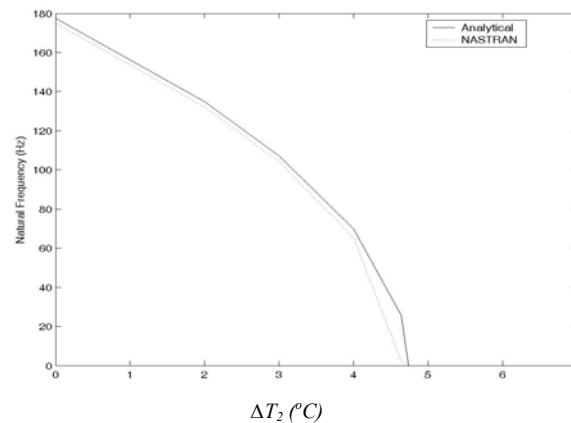


Fig 3.2 Natural Frequency Vs Temperature for aspect ratio (a/b) = 1 (specimen A).

Table 3.2 Buckling temperatures for the rectangular panels of aspect ratio 1, 2 and 7.2 (specimens A, B and C), with in-plane edge constraints.

Specimen	Dimensions (m) and aspect ratio (a/b)	Buckling temperature ($^{\circ}C$)		
		Analytical	in-house FEM Formulation	NASTRAN
A	$a = 0.25, b = 0.25$ $h = 0.00232, (a/b)=1$	4.74	4.7	4.64
B	$a = 1.0, b = 0.50$ $h = 0.007, (a/b)=2$	6.74	6.655	6.8
C	$a = 0.36, b = 0.05$ $h = 0.0011, (a/b)=7.2$	13.58	13.55	13.34

3.2. Effect of Parabolic Temperature Distribution (without in-plane edge constraints) over simply supported rectangular panels of aspect ratio 1, 2 and 7.2 (specimens A, B and C)

3.2.1 Thermal stress distribution due to parabolic temperature distribution

The mid-plane stress resultants N_{xT} , N_{yT} and N_{xyT} due to parabolic temperature distribution (given by equation (1.7) of Chapter 1) over a panel with simply supported edges (*without in-plane edge constraints*) are defined by the following equation

$$N_{xT} = C\alpha Eha^2 \Delta T_1 \left(\frac{x}{a} \right)^2 \left(\frac{x}{a} - 1 \right)^2 \left(\frac{12y^2}{b^4} - \frac{12y}{b^3} + \frac{2}{b^2} \right) \quad (3.2)$$

$$N_{yT} = C\alpha Eha^2 \Delta T_1 \left(\frac{12x^2}{a^4} - \frac{12x}{a^3} + \frac{2}{a^2} \right) \left(\frac{y}{b} \right)^2 \left(\frac{y}{b} - 1 \right)^2 \quad (3.3)$$

$$N_{xyT} = -C\alpha Eha^2 \Delta T_1 \left(\frac{4x^3}{a^4} - \frac{6x^2}{a^3} + \frac{2x}{a^2} \right) \left(\frac{4y^3}{b^4} - \frac{6y^2}{b^3} + \frac{2y}{b^2} \right) \quad (3.4)$$

The variation of normal stress resultants N_{xT} and N_{yT} due to parabolic temperature distribution over the panel of aspect ratio ($a/b = 1$) is shown in Figs 3.3(a) & 3.3(b). The corresponding variation of shear stress resultant N_{xyT} is shown in Fig 3.3(c). Note that these stress resultants vanish accordingly at the panel boundaries, to conform with the condition that no in-plane edge loads arise at the panel edges. (If in-plane edge constraints are present then additional edge loads N_{xo} and N_{yo} will result from thermal effects).

3.2.2 Effect of Parabolic Temperature distribution on flutter boundary (without in-plane edge constraints) of simply supported rectangular panels with airflow along x-direction (edge a, $\theta = 0$)

For rectangular panels of aspect ratios 1, 2 and 7.2 (specimens A, B and C) on simply supported edges, the critical parameters are calculated for various values of parabolic temperature profile amplitude ΔT_1 (in degrees centigrade). The thermal effects on the critical parameters (critical dynamic pressure, critical velocity, critical Mach number) due to the parabolic temperature distribution over the specimen panels are shown in Figs 3.4, 3.5 and 3.6.

The three regions shown in Fig 3.4 are characterized by the value of eigenvalue ($-\gamma^2$).

Region	$-\gamma^2$	Type of Motion
1	Real & positive	Steady oscillation, $\omega = \gamma_I$
2	Complex	Complex roots $\pm(\gamma_r + j\gamma_I)$, one root lead to oscillating, divergent panel motion, $\gamma_r > 0$
3	Negative	Exponential divergence, $\gamma_r > 0$ and $\gamma_I = 0$

In region 1, there is no flutter. *i.e.*, the panel oscillation is stable. In region 2, the panel is dynamically unstable. In region 3, the panel is buckled, *i.e.*, the panel is statically unstable. In this region, the panel undergoes indefinite exponential increase of displacements, till structural failure, without any oscillatory motion (divergence).

These three regions are separated by two boundaries. The first is the buckling loop, which is the locus of points for which eigenvalues vanish *i.e.* $-\gamma^2 = 0$. The second is the flutter boundary, which is the locus of points at which two frequencies coalesce. The point of tangency of the flutter boundary with the buckling loop represents the lowest value of q_{cr} associated with this panel configuration.

The results obtained from analytical and in-house FEM are in good agreement with each other. The results obtained from NASTRAN are in good agreement with analytical and in-house FEM code upto the corresponding static buckling temperature (with parabolic temperature profile and edges free of in-plane constraints). Beyond this temperature it is

observed that the critical Mach number values obtained by NASTRAN fall more sharply with temperature than those obtained by analytical and in-house FEM code. Similar results are generated also for panels of aspect ratios 2 and 7.2 (specimens B and C). These results are given graphically in Fig 3.5-3.6.

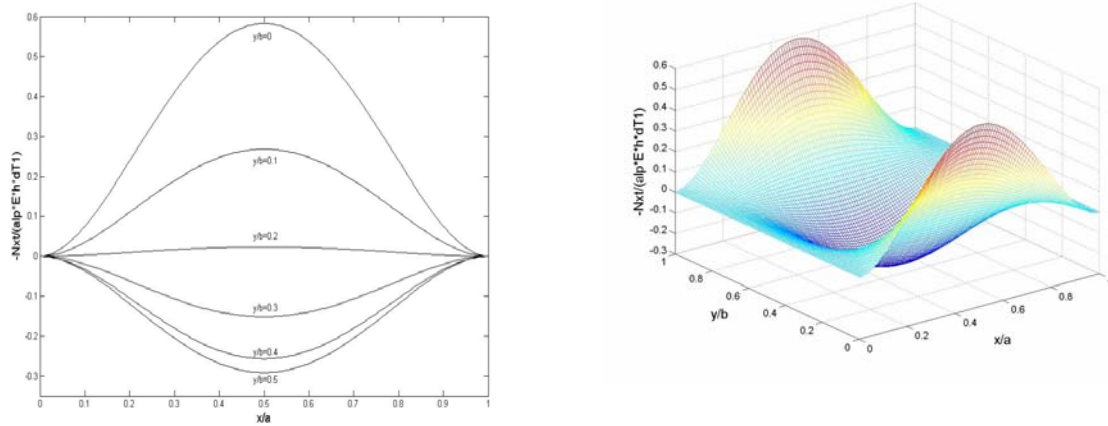


Fig 3.3.(a) Normal stress resultant N_{xT} for a square panel subjected to parabolic Temperature distribution.

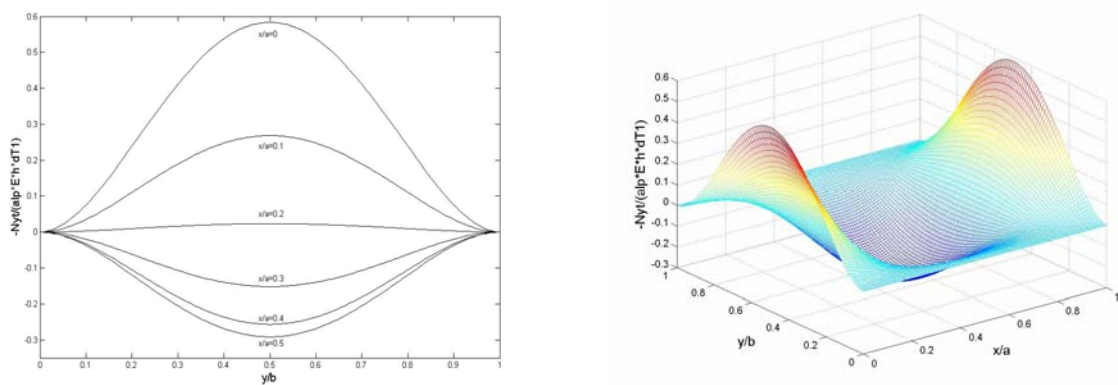


Fig 3.3.(b) Normal stress resultant N_{yT} for a square panel subjected to parabolic temperature distribution.

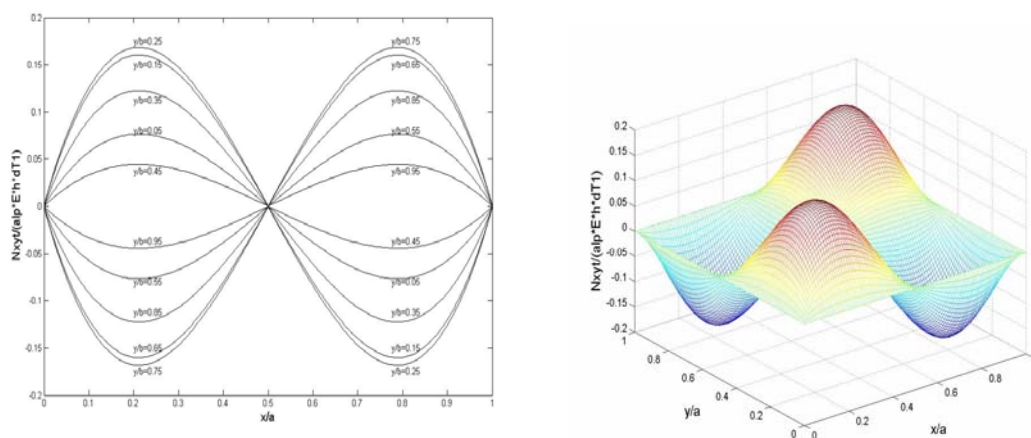


Fig 3.3.(c) Shear stress resultant N_{xyT} for a square panel subjected to parabolic temperature distribution.

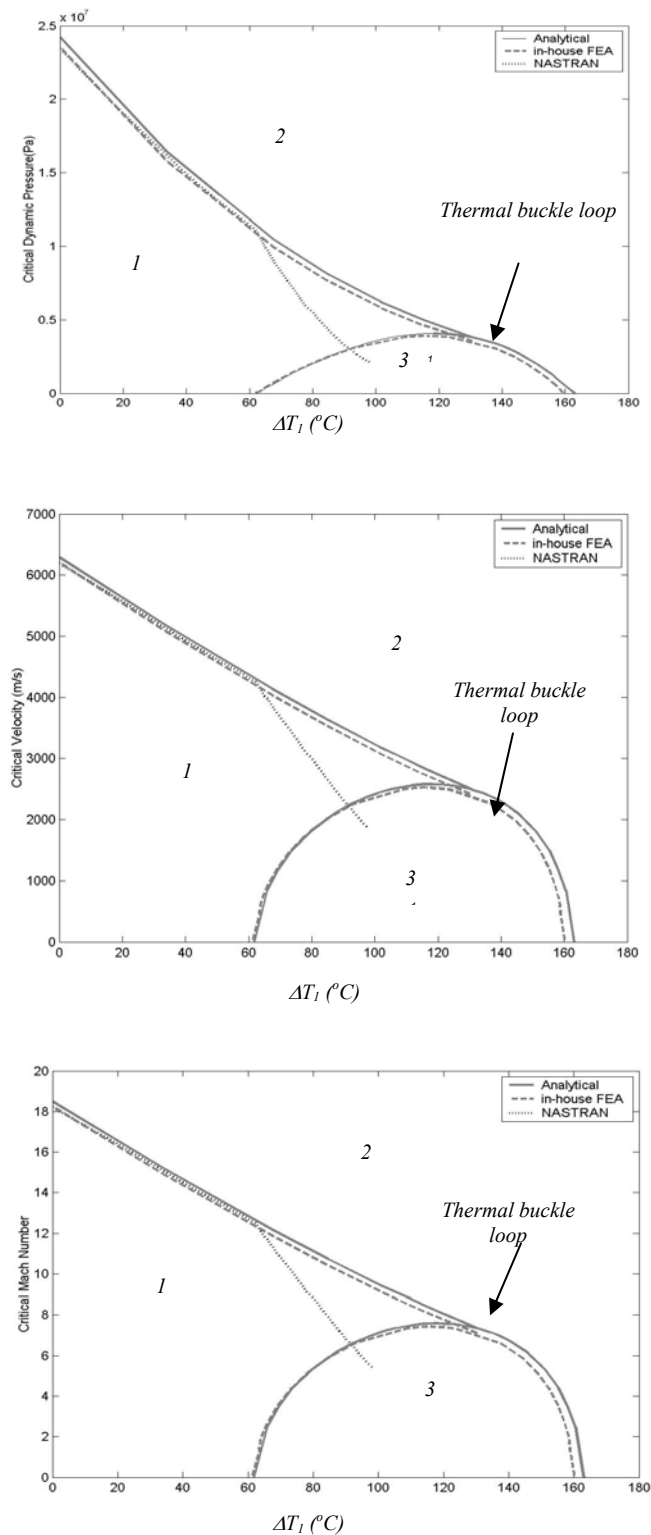


Fig 3.4 Variation of Critical Parameters (Critical Dynamic pressure q_{cr} (Pa), Critical Velocity V_{cr} (m/s) and Critical Mach number M_{cr}) due to parabolic temperature distribution (without in-plane edge constraints) over the simply supported square aluminium panel (specimen A). Flow along edge a . Air Density assumed is 1.225 kg/m^3 .

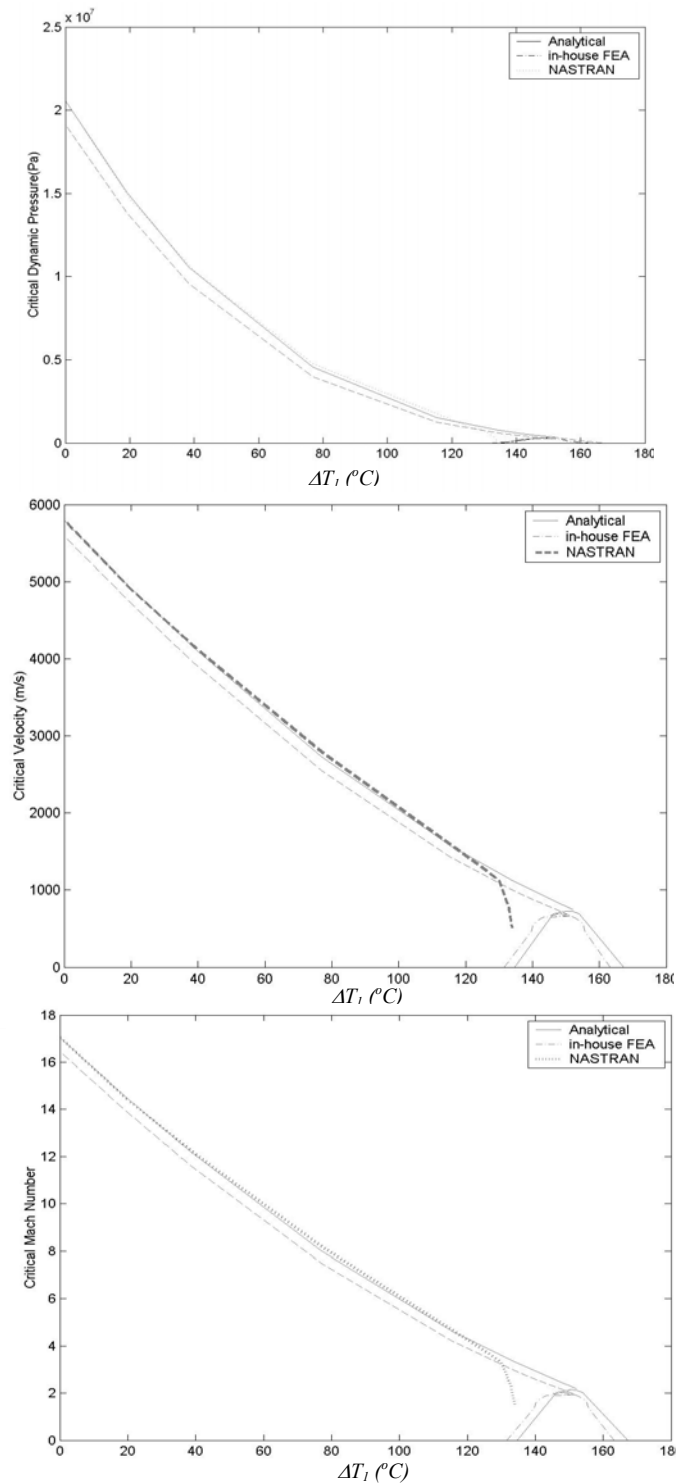


Fig 3.5 Variation of Critical parameters (Critical Dynamic pressure q_{cr} (Pa), Critical Velocity V_{cr} (m/s) and Critical Mach number M_{cr}) due to parabolic temperature distribution (without in-plane edge constraints) for simply supported panel of aspect ratio $a/b=2$ (specimen B). Flow along x -direction (edge 'a'). Air density assumed 1.225 kg/m^3 .

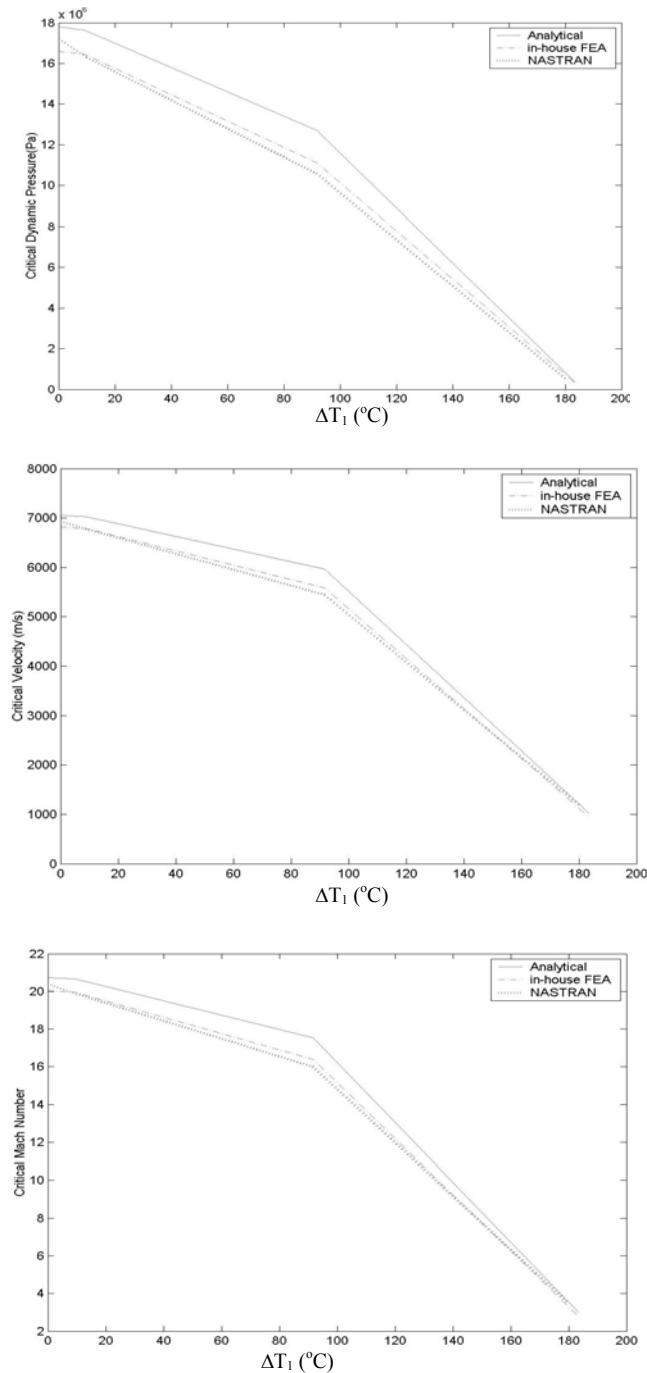


Fig 3.6 Variation of Critical parameters (Critical Dynamic pressure q_{cr} (Pa), Critical Velocity V_{cr} (m/s) and Critical Mach number M_{cr}) due to parabolic temperature distribution (without in-plane edge constraints) for simply supported panel of aspect ratio $a/b=7.2$ (specimen C). Flow along x -direction (edge a). Air density assumed 0.715 kg/m^3 .

3.2.3. Effect of flow direction on the flutter boundary

The variation of critical parameters with flow direction and thermal conditions for the simply supported rectangular panels (specimens A, B and C) with the parabolic thermal profile and edges free of in-plane constraints is investigated by analytical and in-house finite element

method. The results are presented in Tables 3.3-3.5. The graphical representation of the variation of critical parameters with flow angle is presented in Figs 3.7-3.9.

Table 3.3.a Variation of Critical Dynamic pressure (for specimen A) with various parabolic temperature profile and flow angles at air density $\rho_{air} = 1.225 \text{ kg/m}^3$.

Thermal profile parameter $\psi, \Delta T_1$	Critical Dynamic Pressure $q_{cr} (N/m^2)$				
	$\theta=0^\circ$	$\theta=30^\circ$	$\theta=45^\circ$	$\theta=60^\circ$	$\theta=90^\circ$
$\psi=0, \Delta T_1=0^\circ C$	*24211017.8 **23559692 #23430712.8	*25188342.9 **24744226	*25567121.5 **25213597	*25188342.9 **24744226	*2421017.8 **23559692
$\psi=10, \Delta T_1=34.52^\circ C$	*16423184.7 **15645036 #15196346	*17014836.9 **16352457	*17238392.7 **16625761	*17014836.9 **16352457	*16423184.7 **15645036
$\psi=25, \Delta T_1=86.31^\circ C$	*8163103.2 **7473143 #4089697	*8385589.3 **7727731	*8464159.9 **7823754	*8385589.3 **7727731	*8163103.2 **7473143
$\psi=40, \Delta T_1=133.26^\circ C$	*3879313.7 **3414272	*3952387.1 **3492808	*3979477.3 **3522122	*3952387.1 **3492808	*3879313.7 **3414272

Table 3.3.b Variation of Critical velocity (for specimen A) with various parabolic temperature profile and flow angles at air density $\rho_{air} = 1.225 \text{ kg/m}^3$.

Thermal profile parameter $\psi, \Delta T_1$	Critical Velocity $V_{cr} (m/s)$				
	$\theta=0^\circ$	$\theta=30^\circ$	$\theta=45^\circ$	$\theta=60^\circ$	$\theta=90^\circ$
$\psi=0, \Delta T_1=0^\circ C$	*6287.145 **6202 #6185	*6412.786 **6356	*6460.82 **6416	*6412.786 **6356	*6287.145 **6202
$\psi=10, \Delta T_1=34.52^\circ C$	*5178.162 **5054 #4981	*5270.61 **5167	*5305.121 **5210	*5270.61 **5167	*5178.162 **5054
$\psi=25, \Delta T_1=86.31^\circ C$	*3650.69 **3493 #2584	*3700.102 **3552	*3717.396 **3574	*3700.102 **3552	*3650.69 **3493
$\psi=40, \Delta T_1=133.26^\circ C$	*2516.66 **2361	*2540.25 **2388	*2548.94 **2398	*2540.25 **2388	*2516.66 **2361

Table 3.3.c Variation of Critical Mach number (for specimen A) with various parabolic temperature profile and flow angles at air density $\rho_{air} = 1.225 \text{ kg/m}^3$.

Thermal profile parameter $\psi, \Delta T_1$	Critical Mach number M_{cr}				
	$\theta=0^\circ$	$\theta=30^\circ$	$\theta=45^\circ$	$\theta=60^\circ$	$\theta=90^\circ$
$\psi=0, \Delta T_1=0^\circ C$	*18.492 **18.24 #18.19	*18.86 **18.69	*19.002 **18.87	*18.86 **18.69	*18.492 **18.24
$\psi=10, \Delta T_1=34.52^\circ C$	*15.23 **14.86471 #14.65	*15.5 **15.19706	*15.6 **15.32353	*15.5 **15.19706	*15.23 **14.86
$\psi=25, \Delta T_1=86.31^\circ C$	*10.74 **10.27 #7.6	*10.88 **10.45	*10.93 **10.51	*10.88 **10.45	*10.74 **10.27
$\psi=40, \Delta T_1=133.26^\circ C$	*7.41 **6.94	*7.47 **7.024	*7.5 **7.05	*7.47 **7.023	*7.41 **6.94

*Results obtained by analytical formulation; **Results obtained by in-house FEM code, # Results obtained by NASTRAN which predicts steeper fall in critical values with temperature beyond buckling point, as shown in Fig 3.4.

Table 3.4.a Variation of Critical Dynamic Pressure (for specimen B) with various parabolic temperature profiles and flow angles at air density $\rho_{air} = 1.225 \text{ kg/m}^3$.

Thermal profile parameter $\psi, \Delta T_1$	Critical Dynamic Pressure q_{cr} (N/m^2)				
	$\theta=0^0$	$\theta=30^0$	$\theta=45^0$	$\theta=60^0$	$\theta=90^0$
$\psi=0, \Delta T_1=0^0C$	*20567757 **19160010 #20586741	*25543582 **24079151	*33777887 **32416945	*50362275 **49833245	*160847317.0 **167015991.01
$\psi=10, \Delta T_1=19.25^0C$	*14992024 **13807896 #14682125	*18855496 **17531281	*25439138 **24033089	*39443799 **38332652	*155092730.7 **151283001.80
$\psi=20, \Delta T_1=38.5^0C$	*10541236 **9575896 #10366560	*13419027 **12287633	*18465686 **17133782	*29778784 **28363665	*149392407.1 **147115152.4

Table 3.4.b Variation of Critical Velocity (for specimen B) with various parabolic temperature profiles and flow angles at air density $\rho_{air} = 1.225 \text{ kg/m}^3$.

Thermal profile parameter $\psi, \Delta T_1$	Critical Velocity V_{cr} (m/s)				
	$\theta=0^0$	$\theta=30^0$	$\theta=45^0$	$\theta=60^0$	$\theta=90^0$
$\psi=0, \Delta T_1=0^0C$	*5794.826 **5593 #5797.50	*6457.848 **6270	*7426.141 **7275	*9067.752 **9020	*16205.18 **16513.00
$\psi=10, \Delta T_1=19.25^0C$	*4947.401 **4748 #4896	*5548.377 **5350	*6444.632 **6264	*8024.839 **7911	*15912.66 **15716.00
$\psi=20, \Delta T_1=38.5^0C$	*4148.516 **3954 #4114	*4680.664 **4479	*5490.725 **5289	*6972.691 **6805	*15617.49 **15498.00

Table 3.4.c Variation of Critical Mach number (for specimen B) with various parabolic temperature profiles and flow angles at air density $\rho_{air} = 1.225 \text{ kg/m}^3$.

Thermal profile parameter $\psi, \Delta T_1$	Critical Mach number M_{cr}				
	$\theta=0^0$	$\theta=30^0$	$\theta=45^0$	$\theta=60^0$	$\theta=90^0$
$\psi=0, \Delta T_1=0^0C$	*17.04361 **16.45 #17.05	*18.99367 **18.44118	*21.84159 **21.39706	*26.66986 **26.52941	*47.66 **48.57
$\psi=10, \Delta T_1=19.25^0C$	*14.55118 **13.96471 #14.4	*16.31875 **15.73529	*18.9548 **18.42353	*23.60247 **23.26765	*46.80 **46.22
$\psi=20, \Delta T_1=38.5^0C$	*12.20152 **11.62941 #12.1	*13.76666 **13.17353	*16.14919 **15.55588	*20.50792 **20.01471	*45.93 **45.58

*Results obtained by analytical formulation; **Results obtained by in-house FEM code, # Results obtained by NASTRAN

Table 3.5.a Variation of Critical Dynamic Pressure (for specimen C) with various parabolic temperature profiles and flow angles at air density $\rho_{air} = 0.715 \text{ kg/m}^3$.

Thermal profile parameter $\psi, \Delta T_1$	Critical Dynamic pressure $q_{cr} (N/m^2)$			
	$\theta=0^\circ$	$\theta=30^\circ$	$\theta=45^\circ$	$\theta=60^\circ$
$\psi=0, \Delta T_1=0^\circ C$	*17786384 **16594066 #17201565.4	*23686262.99 **22108692	*35426862.34 **33091502	*70180191.91 **65657272
$\psi=100, \Delta T_1=36.65^\circ C$	*17448063.93 **16283768	*23237078.31 **21694566	*34760355.47 **32468472	*68874679.96 **64432448
$\Delta T_1=40^\circ C$	#13839999.03			
$\Delta T_1=140^\circ C$	#3459999.758			
$\psi=400, \Delta T_1=146.61^\circ C$	*2507478.86 **1882961	*3350547.483 **2520026	*5021926.04 **3787721	*9942181.482 **7544979

Table 3.5.b Variation of Critical Velocity (for specimen C) with various parabolic temperature profiles and flow angles at air density $\rho_{air} = 0.715 \text{ kg/m}^3$.

Thermal profile parameter $\psi, \Delta T_1$	Critical velocity $V_{cr} (m/s)$			
	$\theta=0^\circ$	$\theta=30^\circ$	$\theta=45^\circ$	$\theta=60^\circ$
$\psi=0, \Delta T_1=0^\circ C$	*7053.519 **6813 #6936.6	*8139.74 **7864	*9954.71 **9621	*14011.004 **13552
$\psi=100, \Delta T_1=36.65^\circ C$	*6986.112 **6749	*8062.18 **7790	*9860.62 **9530	*13880.07 **13425
$\Delta T_1=40^\circ C$	#6222			
$\Delta T_1=140^\circ C$	#3111			
$\psi=400, \Delta T_1=146.61^\circ C$	*2648.38 **2295	*3061.4 **2655	*3747.98 **3255	*5273.55 **4594

Table 3.5.c Variation of Critical Mach number (for specimen C) with various parabolic temperature profiles and flow angles at air density $\rho_{air} = 0.715 \text{ kg/m}^3$.

Thermal profile parameter $\psi, \Delta T_1$	Critical Mach number M_{cr}			
	$\theta=0^\circ$	$\theta=30^\circ$	$\theta=45^\circ$	$\theta=60^\circ$
$\psi=0, \Delta T_1=0^\circ C$	*20.75 **20.04 #20.40	*23.94 **23.12941	*29.28 **28.29706	*41.21 **39.85882
$\psi=100, \Delta T_1=36.65^\circ C$	*20.55 **19.85	*23.71 **22.91176	*29.002 **28.02941	*40.82 **39.48529
$\Delta T_1=40^\circ C$	#18.3			
$\Delta T_1=140^\circ C$	#9.15			
$\psi=400, \Delta T_1=146.61^\circ C$	*7.79 **6.75	*9.004 **7.808824	*11.023 **9.573529	*15.51 **13.51176

*Results obtained by analytical formulation; **Results obtained by in-house FEM code, # Results obtained by NASTRAN

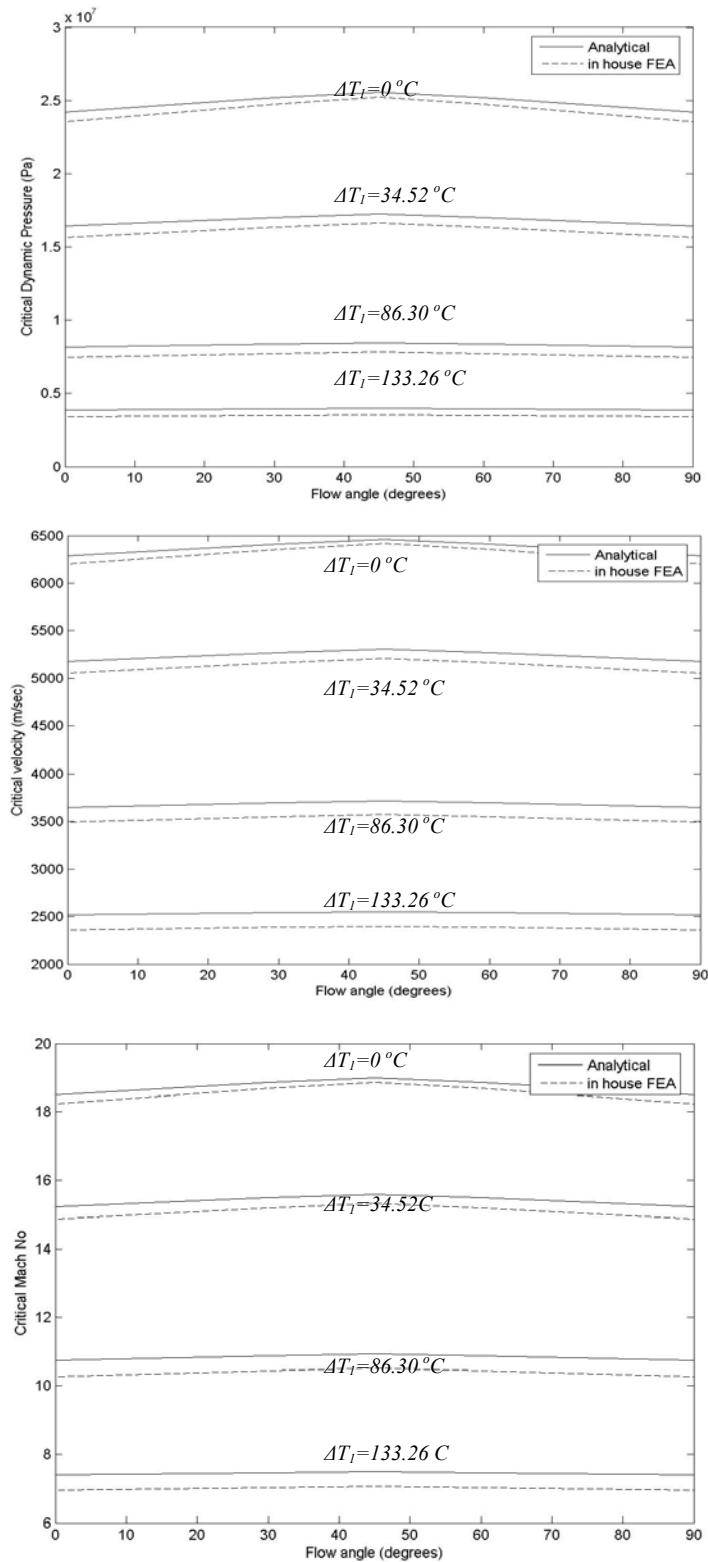


Fig 3.7 Variation of Critical Parameters (Critical Dynamic pressure q_{cr} (Pa), Critical Velocity V_{cr} (m/s) and Critical Mach number M_{cr}) for various flow angles (in degrees) with parabolic temperature distribution over simply supported square panel (specimen A). Air Density assumed is 1.225 kg/m^3 .

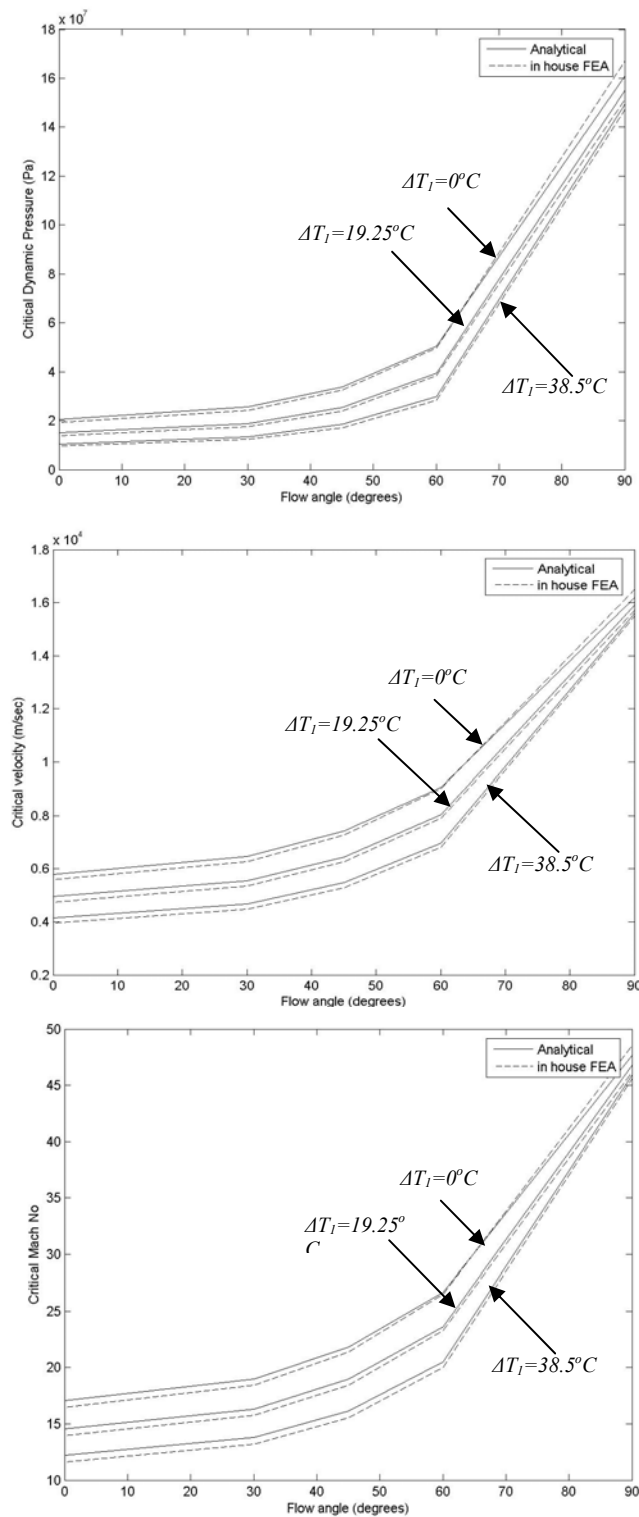


Fig 3.8 Variation of critical parameters (Critical Dynamic pressure q_{cr} (Pa), Critical Velocity V_{cr} (m/s) and Critical Mach number M_{cr}) for various flow angles with parabolic temperature distribution over simply supported panel of aspect ratio =2 (specimen B). Air density assumed is 1.225 kg/m^3 .

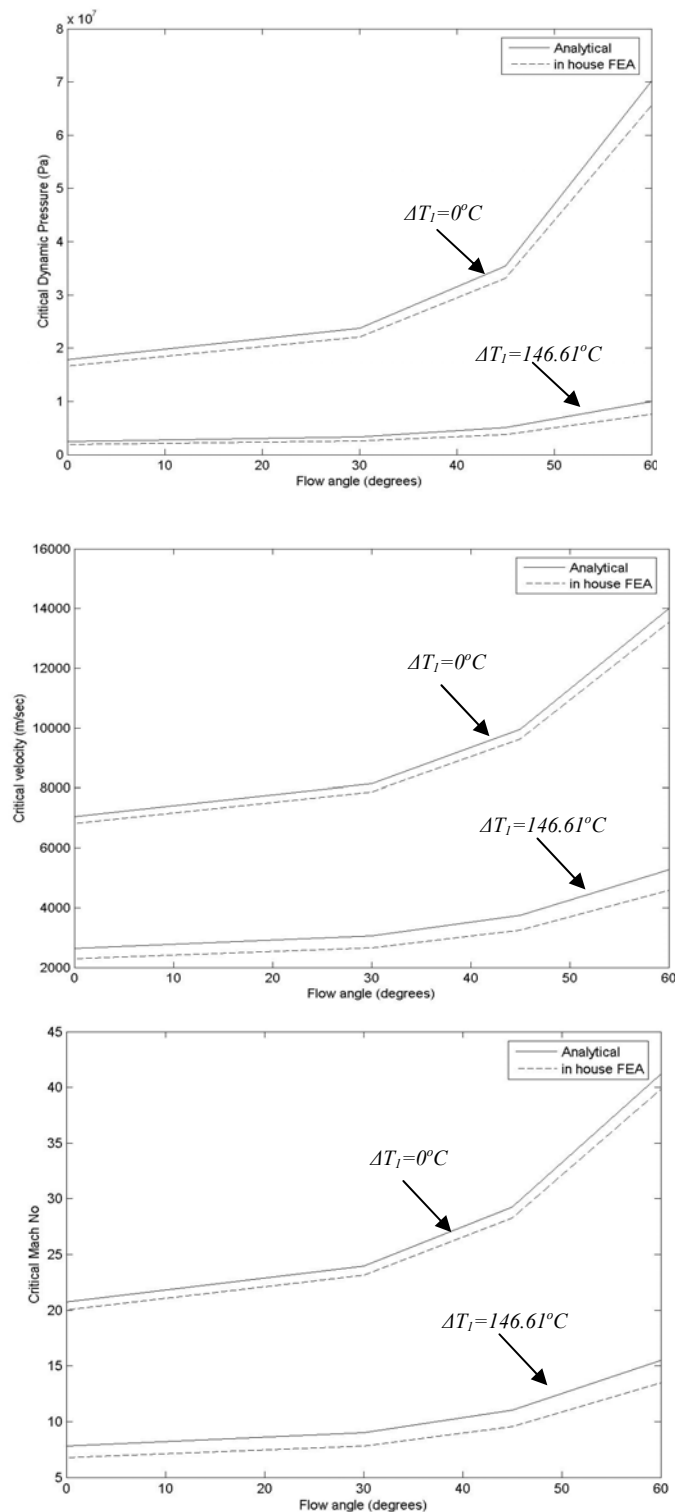


Fig 3.9 Variation of critical parameters (Critical Dynamic pressure q_{cr} (Pa), Critical Velocity V_{cr} (m/s) and Critical Mach number M_{cr}) for various flow angles with parabolic temperature distribution over simply supported panel of aspect ratio =7.2 (specimen C). Air density assumed 0.715 kg/m^3 .

3.3. Effect of Uniform Edge Loads due to edge constraints on thermal expansion on the flutter boundary of rectangular panels

In-plane edge loading per unit edge length, N_{x0} and N_{y0} on the panel can develop from the in-plane edge constraints to thermal expansion. Panels with immovable hinged supports can generate such edge loads. The effects of such edge loading on the flutter boundary of panels with various thermal profiles have been studied.

3.3.1. Effect of Uniform Edge Loading due to edge constraint on thermal expansion with flow along x -direction (edge a , $\theta = 0$)

Variation of critical parameters (critical dynamic pressure, critical velocity, critical Mach number) due to the effects of edge loading from in-plane edge constraints on thermal expansion for rectangular panels is shown in Figs 3.10, 3.11 and 3.12. The flow is restricted to be along edge a . The results are plotted for different temperatures (ΔT_2) that generate the edge loads. It must be noted that in analytical and in-house FEM code results are generated by taking the edge loads (N_x , N_y , N_{xy}) as given in equation (1.8). For the NASTRAN model, only constant temperature profiles are simulated over the panel and all the in-plane degrees of freedom at the panel edges are constrained.

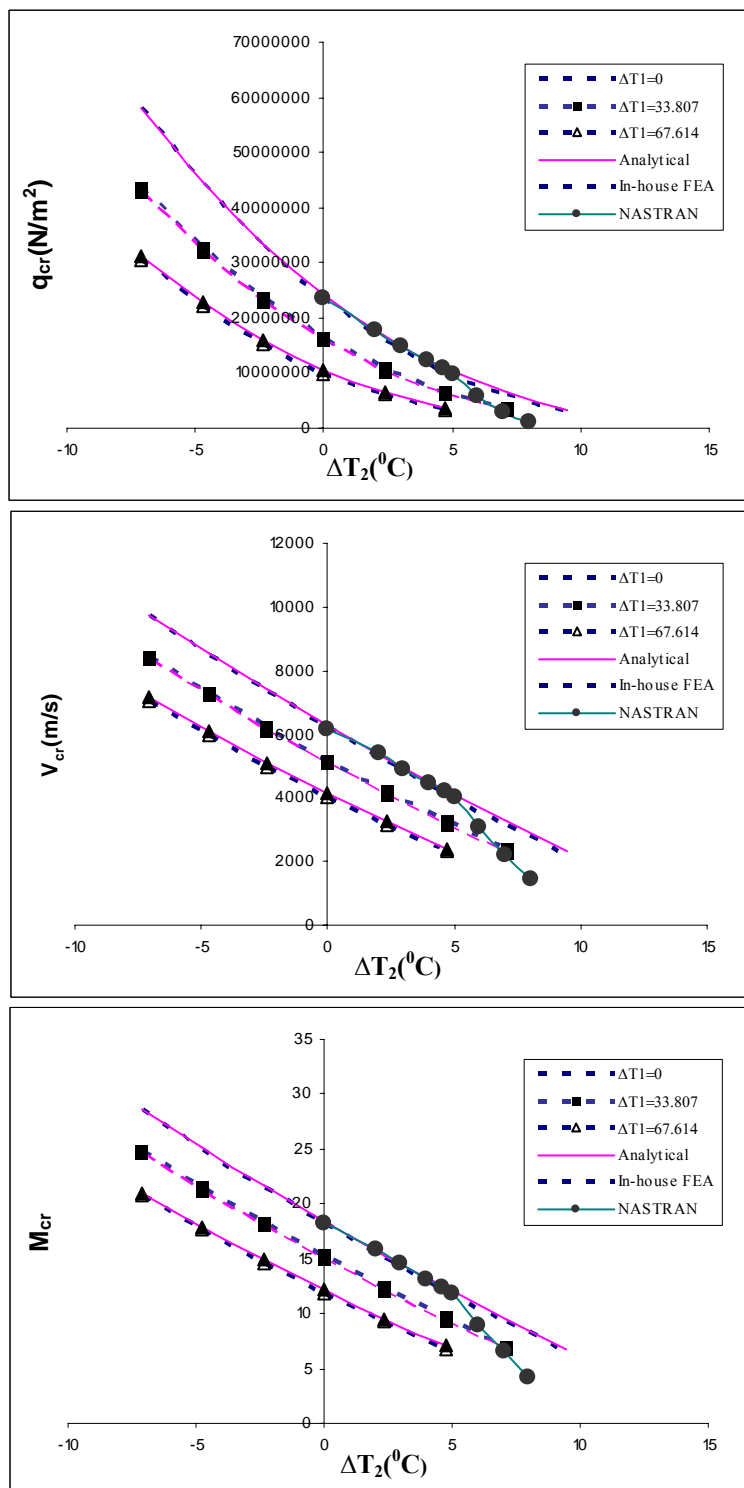


Fig 3.10 Variation of Critical parameters (Critical Dynamic pressure q_{cr} (Pa), Critical Velocity V_{cr} (m/s) and Critical Mach number M_{cr}) for specimen A with the effects of edge loading from in-plane edge constraints on thermal expansion. Flow along x-direction (edge a). Air Density assumed is 1.225 kg/m^3 .

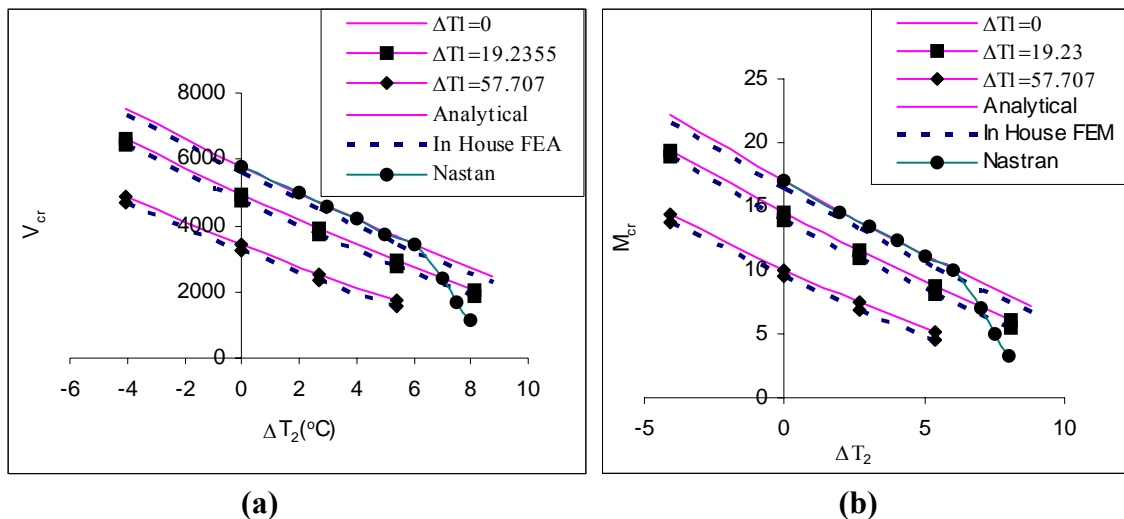


Fig 3.11 Variation of Critical parameters for specimen B with the effects of edge loading from in-plane edge constraints on thermal expansion. Flow along x -direction (edge a). Air Density assumed is 1.225 kg/m^3 . a) Critical velocity b) Critical Mach number.

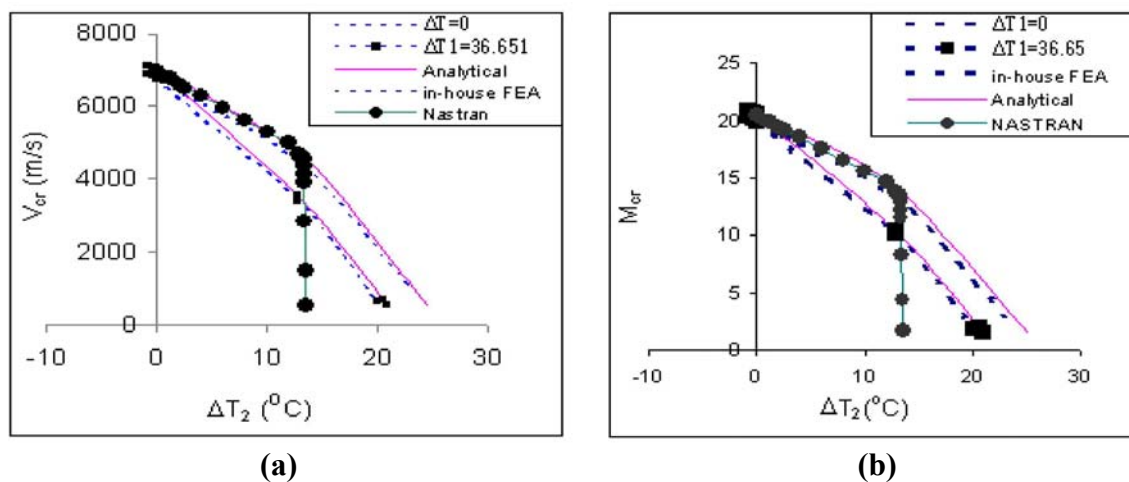


Fig 3.12 Variation of Critical parameters for specimen C with the effects of edge loading from in-plane edge constraints on thermal expansion. Flow along x -direction (edge a). Air Density assumed is 0.715 kg/m^3 . a) Critical velocity b) Critical Mach number.

3.3.2. Effect of flow direction on the flutter boundary of panels with various thermal profiles and in-plane edge constraints

The effect of flow direction on the flutter boundary of panels with various thermal profiles and in-plane edge constraints are studied. Results for the various specimen panels for two different flow angles for each of them are presented in Figs 3.13 to 3.15. For a square panel (specimen A) the results are same for $\theta = 30^\circ$ and $\theta = 60^\circ$, showing symmetry about the direction of $\theta = 45^\circ$. For rectangular panel, flow along the longer direction is most critical.

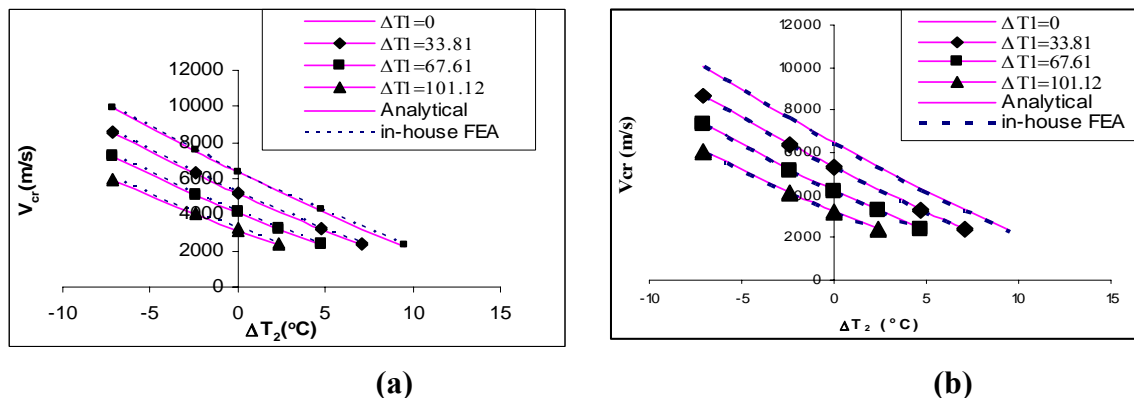


Fig 3.13 Variation of Critical Velocity for specimen A with the effects of edge loading from in-plane edge constraints on thermal expansion for flow angle of a) $\theta = 30^\circ$ & b) $\theta = 45^\circ$. Air Density assumed is 1.225 kg/m^3 .

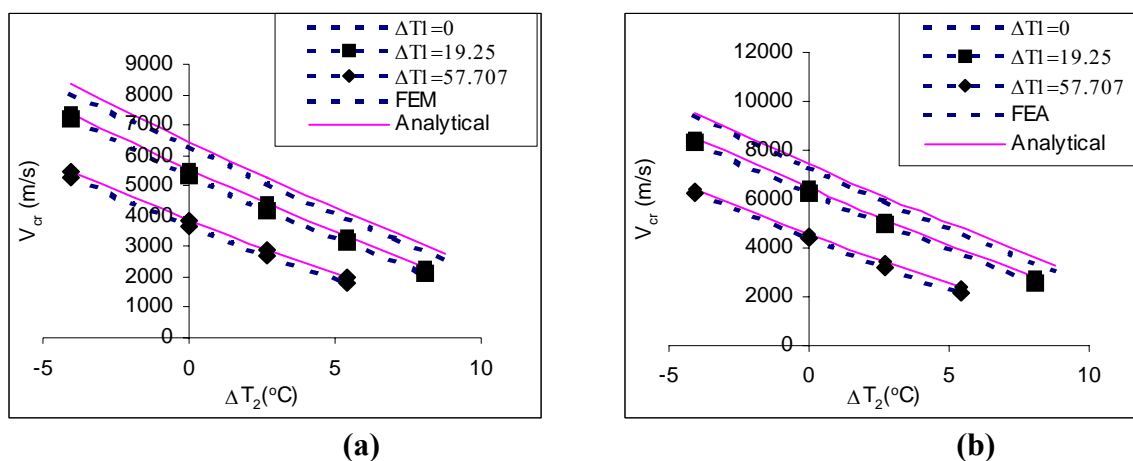


Fig 3.14 Variation of Critical Velocity for specimen B with the effects of edge loading from in-plane edge constraints on thermal expansion for flow angle of a) $\theta = 30^\circ$ & b) $\theta = 45^\circ$. Air Density assumed is 1.225 kg/m^3 .

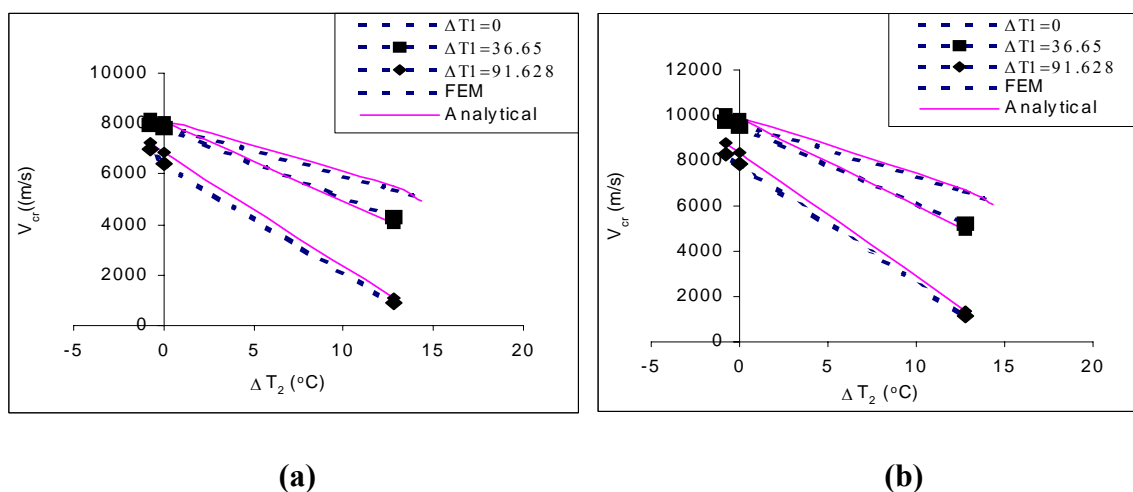


Fig 3.15 Variation of Critical Velocity for specimen C with the effects of edge loading from in-plane edge constraints on thermal expansion for flow angle of a) $\theta = 30^\circ$ & b) $\theta = 45^\circ$. Air Density assumed is 0.715 kg/m^3 .

3.4. Variation of Critical boundary (Mach number) with altitude.

Flutter analysis has been carried out at various altitudes with corresponding air density values for an panel of aspect ratio 7.2 (specimen C, with the dimensions, that forms the typical wing panel). The air density variation with altitude is presented in Fig 3.16. Due to fall in the air density with altitude, an increase in the flutter boundary (and therefore its margin of safety) is expected. The results with parabolic thermal profile (edges free of in-plane constraints) and with uniform thermal profile (with edges constrained against in-plane expansion) are presented respectively in Figs 3.17 and 3.18. Flow is taken along the longer edge a .

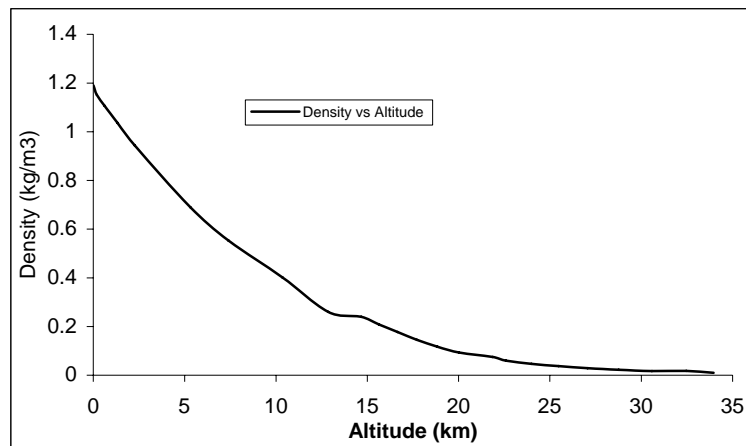


Fig 3.16 Variation of Air density at different Altitude.

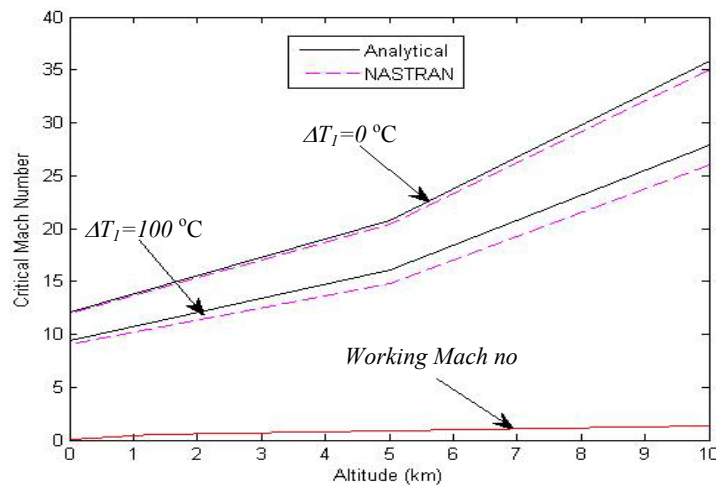


Fig 3.17 The variation of critical Mach number with altitude for simply supported panel of aspect ratio 7.2 (specimen C) under parabolic thermal profile (without in-plane constraints).

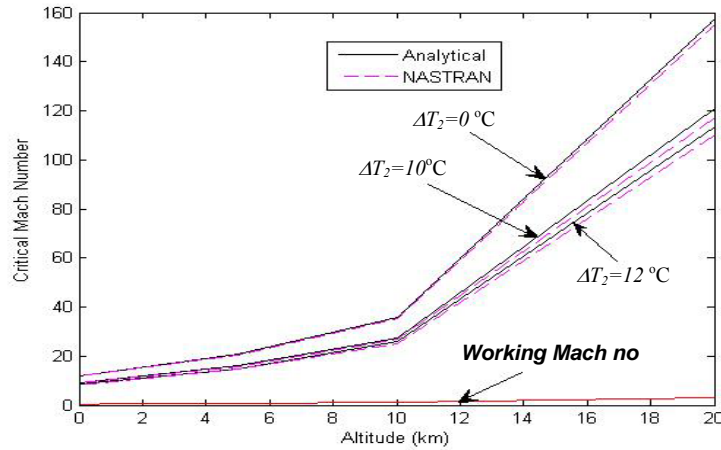


Fig 3.18 The variation of critical Mach number with altitude for panel of aspect ratio 7.2 (specimen C) under uniform temperature. Edges are simply supported with in-plane constraints.

3.5. Effect on mass loading due to Thermal Protection System (TPS) mass

The panels that form the skin of the vehicle will be subjected to harsh aerodynamic environment, especially in the supersonic and hypersonic regimes of flight. The skin will be exposed to high temperatures due to friction with the airflow and also due to solar radiation. There will be a Thermal Protection System (TPS layer), which protects the metallic skin from getting overheated. As TPS material, ceramic is the material is used generally, since it can withstand high temperature gradients. However, it contributes negligible structural stiffness to the panel. Thus the TPS acts as a non-structural mass.

For the flutter analysis the TPS mass is smeared into the panel surface, which is exposed to the flow. For analytical calculation the overall density of the panel is calculated using the equation.

$$\rho_{overall} = \frac{\rho_{mat}h + \rho_{TPS}h_{TPS}}{h} \quad (3.5)$$

where ρ_{mat} and h are respectively the material density and the thickness of the aluminium panel and ρ_{TPS} and h_{TPS} are respectively the material density and thickness of the TPS. For the wing panel (specimen C of $a/b=7.2$) the values are $\rho_{mat}=2800 \text{ kg/m}^3$, $h=0.0011\text{m}$, $\rho_{TPS}=300\text{kg/m}^3$, and $h_{TPS}=0.015\text{m}$. The effective density thus given as $\rho_{overall}=6891 \text{ kg/m}^3$.

Analysis for specimen C with TPS mass simulated is done for the flow along x-direction (edge a, $\theta = 0$). A constant thermal profile with in-plane edge constraints is assumed. Results are generated by NASTRAN only. The results are presented in Fig.3.19. It can be observed that the non-structural TPS mass, uniformly distributed over the panels, does not have any effect on the flutter boundary. However, the natural frequencies and flutter frequencies are lowered.

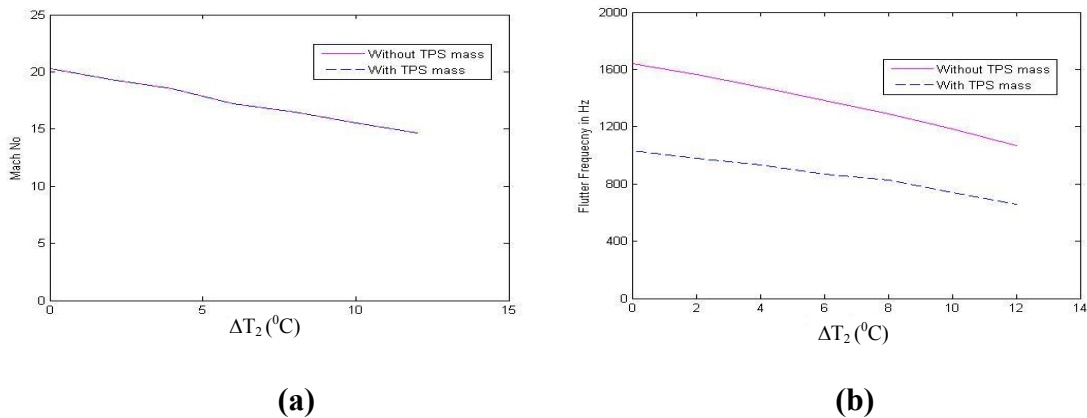


Fig 3.19 (a) Variation of Critical Mach number (b) flutter frequency for specimen C with effects of edge loading from in-plane edge constraints on thermal expansion for flow along x-direction (edge a) with and without TPS mass. Air Density assumed is 0.715 kg/m^3 .

3.6. Chapter Summary and Observations

A numerical study is made to estimate the effects of various thermal profiles and flow directions on the supersonic flutter boundary of panels with simply supported edges. Three different panels specimens with various aspect ratios have been used. Parabolic thermal profiles have been used for edges without in-plane constraints and constant thermal profiles for edges with in-plane edge constraints. A combined thermal profile case with in-plane edge constraints has also been studied. Finally, the effects of altitudes and TPS mass have also been investigated.

This study predicts a sharp fall of the flutter boundary parameters for rectangular panels with temperature rise. Furthermore, for all the cases, the flow along the longer side is most critical (with lowest critical dynamic pressure). The non-structural TPS mass, distributed uniformly, only effects the frequencies, but does not change the flutter boundary.

The results obtained by the analytical method and in-house finite element codes are in good agreement. Results from the analytical formulation, in-house FEM code are in good agreement with those from NASTRAN software till the buckling point, beyond which NASTRAN results indicate a sharper fall of critical values with thermal parameters. Beyond buckling point, NASTRAN considers the analysis as a post buckling geometrical nonlinear problem, whereas the analytical and in-house FEM code continues as a linear analysis.

The high critical Mach numbers predicted by the present analysis based on piston theory aerodynamics only indicate that the specimen panels under the given conditions are extremely stiff, despite the fact that such high Mach numbers do not fall in the regime of piston theory aerodynamics.

Chapter 4

CONCLUSION

4.1 Summary and Observations

The analytical and in-house finite element formulation for supersonic panel flutter analysis of the simply supported rectangular plates is dealt with. The linearized quasi-steady two-dimensional aerodynamic theory (piston theory) is used in conjunction with thin-plate theory to formulate the problem. The panel is subjected to supersonic airflow in arbitrary direction and is associated with a parabolic (with free edges) and uniform temperature distribution (with in-plane edge constraints) over the plate.

The analytical solutions for supersonic panel flutter analysis are obtained by solving the governing differential equation using model superposition method. Piston theory is used for aerodynamic pressure computations. For the in-house finite element formulation a four noded Quadrilateral C^1 continuity plate bending element with three displacement components (transverse displacement w and the slopes about x and y -axes) at each node is used.

The results for different flow direction indicate that the critical dynamic pressure decreases as the flow gets more and more aligned to the longest direction. This implies that the flow along the longer side is most critical. Furthermore the studies on rectangular panels with thermal effects predict a sharp fall of the flutter boundary parameters with temperature rise for various cases of thermal effects, which are as follows.

1. Parabolic temperature distribution over the panel (without in-plane edge constraints).
2. Uniform temperature distribution over the panel (with edge loads that arise from in-plane constraints at the panel edges).
3. Combination of parabolic and uniform temperature distribution over the panel (with in-plane edge constraints).

The variation of critical parameters (critical dynamic pressure/ critical velocity/ critical Mach number) are investigated for the above cases with different flow directions for some specimen aluminium panels of various aspect ratios.

The results obtained by the analytical method and in-house finite element codes are in good agreement. Results from the analytical formulation, in-house FEM code are in good agreement with those from NASTRAN software till the buckling point, beyond which NASTRAN results indicate a sharper fall of critical values with thermal parameters. Beyond buckling point, NASTRAN considers the analysis as a post buckling geometrical nonlinear problem, whereas the analytical and in-house FEM code continues as a linear analysis.

The non-structural TPS mass, distributed uniformly, only affects the frequencies, but does not change the flutter boundary.

The high critical Mach numbers predicted by the present analysis based on piston theory aerodynamics only indicate that the specimen panels under the given conditions are extremely stiff, despite the fact that such high Mach numbers do not fall in the regime of piston theory aerodynamics.

4.2 Scope for future work

The present work is limited to only for the rectangular panels with simply supported edges, with assumed thermal profile. In the actual panels of any supersonic vehicle, in-plane loading can be induced from arbitrary thermal profiles as well as from elastic constraints at the edges connecting to stiffness. Furthermore thermally induced bending effects from thermal gradients across the panel thickness can also be considered for analysis.

Further studies on supersonic flutter analysis including such effects are necessary to arrive at a more reliable and realistic design of panels.

REFERENCES

1. **Fung.Y.C.**, *“Introduction to Aeroelasticity”*, John Willey and sons, Newyork, 1955.
2. **Bisplinghoff.R.L and Ashley.H.**, *“Principles of Aeroelasticity”*, Willey, Newyork, 1962.
3. **Lanchester, F.W.**, *“Torsional Vibration of an Aeroplane”*, Aeronautical Research Committee, R&M.276, Part1, 1916.
4. **Bairstow. L and Fage,A.**, *“Oscillations of the Tail Plane and Body of an Aeroplane in Flight”*, Aeronautical Research Committee, R&M.276, Part2, 1916.
5. **Holt Ashley and Garabed Zartarian.**, *“Piston theory - a new aerodynamic tool for the aeroelatican”*. Journal of the Aeronautical Sciences, vol.23, pg.1109-1118, 1956.
6. **Fung,Y.C.B.**, *“A summary of the theories and Experiments on panel flutter”*. AFOSR TN. 60-224, 1960.
7. **Herman L. Bohon and Sidney C. Dixon**, *“Some Recent Developments in Flutter of Flat Panels”*, Journal of Aircraft, vol.1, pg.280-288, 1964.
8. **Hedgepeth, John M.**, *“Flutter of rectangular simply supported panels at high supersonic speeds”*, Journal of Aeronautical Sciences, vol.24, No 8, pg. 563-573, 1957.
9. **Fralich,R.W.**, *“Post buckling Effects on the Flutter of Simply Supported Rectangular panels at Supersonic Speeds”*, NASA TN-D-1615, 1965.
10. **Ellen, C.H.**, *“Approximate Solutions of Membrane Flutter Problem”*, AIAA Journal, vol.3, pg. 1186-1193, 1965.
11. **Harry G. Schaeffer and Walter L. Heard**, *“Supersonic Flutter of a Thermally Stressed Flat Panel with Uniform Edge loads”*, NASA TN-D-3077, 1965.
12. **Larry L. Erickson**, *“Supersonic Flutter of Flat Rectangular orthotropic Panels Elastically Restrained against Edge Rotation”*, NASA TN-D-3500, 1966.
13. **Zienkiewicz O. C**, *“Finite Element Method for Solid and Structural Mechanics”*, Elsevier, Butterworth Heinemann, 2000.
14. **Timoshenko S.P. and Gere J.M.**, *“Theory of Elastic Stability”*, Second edition , McGraw-Hill International Book Company, 1985.
15. **G.Sander, C.Bon and M.Geradin** *“Finite element analysis of supersonic panel flutter”*, International Journal for Numerical Methods in Engineering, vol.7, pg.379-394, 1973.
16. **Earl A. Thornton**, *“Thermal structures for aerospace applications”*, AIAA Education series, 1996.
17. **S Mukherjee, Deepa N, Avinash R, M Manjuprasad and S Viswanath** *“Analytical investigation of supersonic panel flutter under thermal environment with arbitrary flow direction”*, NAL Project Document ST 0704, March 2007.

18. S Mukherjee, Avinash R and Deepa N “*Investigation of Supersonic Panel Flutter under Thermal Environment with Arbitrary Flow Direction*” International Conference on Theoretical, Applied, Computational and Experimental Mechanics, IIT Kharagpur, India, ICTACEM-2007/Paper No 210.

19. MSC.NASTRAN Combined Documentation 2005.

APPENDIX A

$$\left[\frac{\partial N^b}{\partial \xi} \right] = \left[\left[\frac{\partial N_1^b}{\partial \xi} \right] \left[\frac{\partial N_2^b}{\partial \xi} \right] \left[\frac{\partial N_3^b}{\partial \xi} \right] \left[\frac{\partial N_4^b}{\partial \xi} \right] \right] \quad (\text{A.1})$$

$$\left[\frac{\partial N^b}{\partial \eta} \right] = \left[\left[\frac{\partial N_1^b}{\partial \eta} \right] \left[\frac{\partial N_2^b}{\partial \eta} \right] \left[\frac{\partial N_3^b}{\partial \eta} \right] \left[\frac{\partial N_4^b}{\partial \eta} \right] \right] \quad (\text{A.2})$$

where $\left[\frac{\partial N_i^b}{\partial \xi} \right]$ and $\left[\frac{\partial N_i^b}{\partial \eta} \right]$ are given as

$$\left[\frac{\partial N_i^b}{\partial \xi} \right] = \frac{1}{8} \begin{bmatrix} (\xi_i + 1)(\eta\eta_i + 1)(2 + \xi\xi_i + \eta\eta_i - \xi^2 - \eta^2) + (\xi\xi_i + 1)(\eta\eta_i + 1)(\xi_i - 2\xi) \\ a^e \xi_i (2(\xi\xi_i - 1) + (\xi\xi_i + 1)(\xi_i - 1)) (\xi\xi_i + 1)(\eta_o + 1) \\ b^e \eta_i (\xi_i + 1)(\eta\eta_i + 1)^2 (\eta\eta_i - 1) \end{bmatrix}^T$$

$$\left[\frac{\partial N_i^b}{\partial \eta} \right] = \frac{1}{8} \begin{bmatrix} (\xi\xi_i + 1)(\eta_i + 1)(2 + \xi\xi_i + \eta\eta_i - \xi^2 - \eta^2) + (\xi\xi_i + 1)(\eta\eta_i + 1)(\eta_i - 2\eta) \\ a^e \xi_i ((\xi\xi_i + 1)^2 (\xi\xi_i - 1)) (\eta_i + 1) \\ b^e \eta_i (2(\eta_i + 1)(\eta\eta_i - 1) + (\eta\eta_i + 1)(\eta_i - 1)) (\eta\eta_i + 1)(\xi_i + 1) \end{bmatrix}^T$$

Gaussian quadrature rule for two-dimensional integration.

$$I = \int_{-1}^1 \int_{-1}^1 \varphi(\xi, \eta) d\xi d\eta = \sum_m \sum_n w_m w_n \varphi(\xi_m, \eta_n)$$

where ξ_m, η_n, w_m and w_n are given as

Order	Location ξ_m, η_n	Weight w_m and w_n
1	0	2
2	± 0.577350269189626	1
3	± 0.774596669241483	0.5555555555555556
	0	0.8888888888888889
4	± 0.861136311594053	0.347854845137454
	± 0.339981043584856	0.652145154862546
5	± 0.906179845938664	0.236926885056189
	± 0.538469310105683	0.478628670499366
6	0	0.5688888888888889
	± 0.932469514203152	0.171324492379179
	± 0.661209386466265	0.360761573048139
	± 0.238619186083197	0.467913934572691

The expression for $[K^e]$ in equation (1.20), is

$$[K^e] = D a^e b^e \left([K_1] + \mu [K_2] + \frac{(1-\mu)}{2} [K_3] \right) \quad (\text{A.3})$$

where $[K_1]$, $[K_2]$ and $[K_3]$ are expressed in equation (A.3a), (A.3b) and (A.3c) respectively

[K₁] = (1/6) x

$\frac{6}{a^4} + \frac{6}{b^4}$	$\frac{6}{a^3}$	$\frac{6}{b^3}$	$\frac{3}{a^4} + \frac{6}{b^4}$	$\frac{3}{a^3}$	$\frac{6}{b^3}$	$-\frac{6}{a^4} + \frac{6}{b^4}$	$\frac{6}{a^3}$	$\frac{3}{b^3}$	$-\frac{3}{a^4} + \frac{3}{b^4}$	$\frac{3}{a^3}$	$\frac{3}{b^3}$
$\frac{6}{a^3}$	$\frac{8}{a^2}$	0	$\frac{3}{a^3}$	$\frac{4}{a^2}$	0	$-\frac{6}{a^3}$	$\frac{4}{a^2}$	0	$-\frac{3}{a^3}$	$\frac{2}{a^2}$	0
$\frac{6}{b^3}$	0	$\frac{8}{b^2}$	$-\frac{6}{b^3}$	0	$\frac{4}{b^2}$	$\frac{3}{b^3}$	0	$\frac{4}{b^2}$	$-\frac{3}{b^3}$	0	$\frac{2}{b^2}$
$\frac{3}{a^4} + \frac{6}{b^4}$	$\frac{3}{a^3}$	$-\frac{6}{b^3}$	$\frac{6}{a^4} + \frac{6}{b^4}$	$\frac{6}{a^3}$	$-\frac{6}{b^3}$	$-\frac{3}{a^4} + \frac{3}{b^4}$	$\frac{3}{a^3}$	$-\frac{3}{b^3}$	$-\frac{6}{a^4} + \frac{6}{b^4}$	$\frac{6}{a^3}$	$-\frac{3}{b^3}$
$\frac{3}{a^3}$	$\frac{4}{a^2}$	0	$\frac{6}{a^3}$	$\frac{8}{a^2}$	0	$-\frac{3}{a^3}$	$\frac{2}{a^2}$	0	$-\frac{6}{a^3}$	$\frac{4}{a^2}$	0
$\frac{6}{b^3}$	0	$\frac{4}{b^2}$	$-\frac{6}{b^3}$	0	$\frac{8}{b^2}$	$\frac{3}{b^3}$	0	$\frac{2}{b^2}$	$-\frac{3}{b^3}$	0	$\frac{4}{b^2}$
$-\frac{6}{a^4} + \frac{6}{b^4}$	$-\frac{6}{a^3}$	$\frac{3}{b^3}$	$-\frac{3}{a^4} + \frac{3}{b^4}$	$-\frac{3}{a^3}$	$\frac{3}{b^3}$	$\frac{6}{a^4} + \frac{6}{b^4}$	$-\frac{6}{a^3}$	$\frac{6}{b^3}$	$\frac{3}{a^4} + \frac{6}{b^4}$	$-\frac{3}{a^3}$	$\frac{6}{b^3}$
$\frac{6}{a^3}$	$\frac{4}{a^2}$	0	$\frac{3}{a^3}$	$\frac{2}{a^2}$	0	$-\frac{6}{a^3}$	$\frac{8}{a^2}$	0	$-\frac{3}{a^3}$	$\frac{4}{a^2}$	0
$\frac{3}{b^3}$	0	$\frac{4}{b^2}$	$-\frac{3}{b^3}$	0	$\frac{2}{b^2}$	$\frac{6}{b^3}$	0	$\frac{8}{b^2}$	$-\frac{6}{b^3}$	0	$\frac{4}{b^2}$
$-\frac{3}{a^4} + \frac{3}{b^4}$	$-\frac{3}{a^3}$	$-\frac{3}{b^3}$	$-\frac{6}{a^4} + \frac{3}{b^4}$	$-\frac{6}{a^3}$	$-\frac{3}{b^3}$	$\frac{3}{a^4} + \frac{6}{b^4}$	$-\frac{3}{a^3}$	$-\frac{6}{b^3}$	$\frac{6}{a^4} + \frac{6}{b^4}$	$-\frac{6}{a^3}$	$-\frac{6}{b^3}$
$\frac{3}{a^3}$	$\frac{2}{a^2}$	0	$\frac{6}{a^3}$	$\frac{4}{a^2}$	0	$-\frac{3}{a^3}$	$\frac{4}{a^2}$	0	$-\frac{6}{a^3}$	$\frac{8}{a^2}$	0
$\frac{3}{b^3}$	0	$\frac{2}{b^2}$	$-\frac{3}{b^3}$	0	$\frac{4}{b^2}$	$\frac{6}{b^3}$	0	$\frac{4}{b^2}$	$-\frac{6}{b^3}$	0	$\frac{8}{b^2}$

.....(A.3a)

[K₂] = (1/2) x

$3/(a^{\wedge}2*b^{\wedge}2)$	$3/(b^{\wedge}2*a^{\wedge}2)$	$3/(b^{\wedge}2*a^{\wedge}2)$	$-3/(a^{\wedge}2*b^{\wedge}2)$	$-3/(b^{\wedge}2*a^{\wedge}2)$	0	$-3/(a^{\wedge}2*b^{\wedge}2)$	$-3/(b^{\wedge}2*a^{\wedge}2)$	0	$3/(a^{\wedge}2*b^{\wedge}2)$	0	0
$3/(b^{\wedge}2*a^{\wedge}2)$	0	$6/(a^{\wedge}2*b^{\wedge}2)$	$-3/(b^{\wedge}2*a^{\wedge}2)$	0	0	0	0	0	0	0	0
$3/(b^{\wedge}2*a^{\wedge}2)$	$6/(a^{\wedge}2*b^{\wedge}2)$	0	0	0	0	$-3/(b^{\wedge}2*a^{\wedge}2)$	0	0	0	0	0
$-3/(a^{\wedge}2*b^{\wedge}2)$	$-3/(b^{\wedge}2*a^{\wedge}2)$	0	$3/(a^{\wedge}2*b^{\wedge}2)$	$-3/(b^{\wedge}2*a^{\wedge}2)$	0	$3/(a^{\wedge}2*b^{\wedge}2)$	0	0	$-3/(a^{\wedge}2*b^{\wedge}2)$	0	$3/(b^{\wedge}2*a^{\wedge}2)$
$-3/(b^{\wedge}2*a^{\wedge}2)$	0	0	$3/(b^{\wedge}2*a^{\wedge}2)$	0	$-6/(a^{\wedge}2*b^{\wedge}2)$	0	0	0	0	0	0
0	0	0	$-3/(b^{\wedge}2*a^{\wedge}2)$	$-6/(a^{\wedge}2*b^{\wedge}2)$	0	0	0	0	$3/(b^{\wedge}2*a^{\wedge}2)$	0	0
-	0	$-3/(b^{\wedge}2*a^{\wedge}2)$	$3/(a^{\wedge}2*b^{\wedge}2)$	0	0	$3/(a^{\wedge}2*b^{\wedge}2)$	$-3/(b^{\wedge}2*a^{\wedge}2)$	$3/(b^{\wedge}2*a^{\wedge}2)$	$-3/(a^{\wedge}2*b^{\wedge}2)$	$3/(b^{\wedge}2*a^{\wedge}2)$	0
$3/(a^{\wedge}2*b^{\wedge}2)$	0	0	0	0	0	$-3/(b^{\wedge}2*a^{\wedge}2)$	0	$-6/(a^{\wedge}2*b^{\wedge}2)$	$3/(b^{\wedge}2*a^{\wedge}2)$	0	0
$-3/(b^{\wedge}2*a^{\wedge}2)$	0	0	0	0	0	$3/(b^{\wedge}2*a^{\wedge}2)$	0	0	0	0	0
$3/(a^{\wedge}2*b^{\wedge}2)$	0	0	$-3/(a^{\wedge}2*b^{\wedge}2)$	$3/(b^{\wedge}2*a^{\wedge}2)$	$3/(b^{\wedge}2*a^{\wedge}2)$	$-3/(a^{\wedge}2*b^{\wedge}2)$	0	0	$3/(a^{\wedge}2*b^{\wedge}2)$	$-3/(b^{\wedge}2*a^{\wedge}2)$	$-3/(b^{\wedge}2*a^{\wedge}2)$
0	0	0	0	0	0	$3/(b^{\wedge}2*a^{\wedge}2)$	0	0	$-3/(b^{\wedge}2*a^{\wedge}2)$	0	$6/(a^{\wedge}2*b^{\wedge}2)$
0	0	0	$3/(b^{\wedge}2*a^{\wedge}2)$	0	0	0	0	0	$-3/(b^{\wedge}2*a^{\wedge}2)$	$6/(a^{\wedge}2*b^{\wedge}2)$	0

.....(A.3b)

[K₃] = (1/30) x

$15/(b^{e^2} * a^e)$	$15/(a^{e^2} * b^e)$	$-15/(a^{e^2} * b^{e^2})$	$-15/(b^{e^2} * a^e)$	0	$-15/(a^{e^2} * b^{e^2})$	0	$-15/(a^{e^2} * b^e)$	$15/(a^{e^2} * b^{e^2})$	0	0
0	$30/(a * b^e)$	$-15/(b^{e^2} * a^e)$	0	0	0	0	0	0	0	0
$30/(a * b^e)$	0	0	0	0	$-15/(a^{e^2} * b^e)$	0	0	0	0	0
$-15/(b^{e^2} * a^e)$	0	$15/(a^{e^2} * b^{e^2})$	$15/(b^{e^2} * a^e)$	$-15/(a^{e^2} * b^e)$	$15/(a^{e^2} * b^{e^2})$	0	0	$-15/(a^{e^2} * b^{e^2})$	0	$15/(a^{e^2} * b^e)$
0	0	$15/(b^{e^2} * a^e)$	0	$-30/(a * b^e)$	0	0	0	0	0	0
0	0	$-15/(a^{e^2} * b^e)$	$-30/(a * b^e)$	0	0	0	0	$15/(a^{e^2} * b^e)$	0	0
0	$-15/(a^{e^2} * b^e)$	$15/(a^{e^2} * b^{e^2})$	0	0	$15/(a^{e^2} * b^{e^2})$	0	$-15/(b^{e^2} * a^e)$	$-15/(a^{e^2} * b^{e^2})$	$15/(b^{e^2} * a^e)$	0
0	0	0	0	0	$-15/(b^{e^2} * a^e)$	0	0	$15/(b^{e^2} * a^e)$	0	0
0	0	0	0	0	$15/(a^{e^2} * b^e)$	0	0	0	0	0
0	0	$-15/(a^{e^2} * b^{e^2})$	0	$15/(a^{e^2} * b^e)$	$15/(a^{e^2} * b^{e^2})$	0	$-30/(a * b^e)$	0	0	0
0	0	0	0	0	$15/(a^{e^2} * b^{e^2})$	0	0	$15/(a^{e^2} * b^e)$	$-15/(b^{e^2} * a^e)$	$-15/(a^{e^2} * b^e)$
0	0	0	0	0	$15/(b^{e^2} * a^e)$	0	0	$-15/(b^{e^2} * a^e)$	0	$30/(a * b^e)$
0	0	$15/(a^{e^2} * b^e)$	0	0	0	0	0	$-15/(a^{e^2} * b^e)$	$30/(a * b^e)$	0

.....(A.3c)

The aerodynamic load matrices $[K_{qx}^e]$ and $[K_{qy}^e]$ given in equation (1.26) are

$$[K_{qx}] = (1/1260) \times (L \cos(\theta)) \times$$

$175*a^{*}b^{*}b^e$	$-132*b^{*}b^{*}b^e$	$-162*b^e$	$-162*b^e$	$77*a^{*}b^e$	$78*b^{*}b^{*}b^e$	$468*b^e$	$-175*a^{*}b^{*}b^e$	$132*b^{*}b^{*}b^e$	$162*b^e$	$132*b^{*}b^{*}b^e$	$162*b^e$	$-77*a^{*}b^e$	$-78*b^{*}b^{*}b^e$
0	$-42*a^{*}b^{*}b^{*}b^e$	$-77*a^{*}b^e$	$-77*a^{*}b^e$	0	$28*a^{*}b^{*}b^{*}b^e$	$175*a^{*}b^e$	$-56*a^{*}b^{*}b^{*}b^e$	$42*a^{*}b^{*}b^{*}b^e$	$77*a^{*}b^e$	$42*a^{*}b^{*}b^{*}b^e$	$-28*a^{*}b^{*}b^{*}b^e$	$-28*a^{*}b^{*}b^{*}b^e$	$-28*a^{*}b^{*}b^{*}b^e$
$42*a^{*}b^{*}b^{*}b^e$	$-48*b^{*}b^{*}b^e$	$-78*b^{*}b^{*}b^e$	$-78*b^{*}b^{*}b^e$	$28*a^{*}b^{*}b^{*}b^e$	$36*b^{*}b^{*}b^e$	$132*b^{*}b^{*}b^e$	$-42*a^{*}b^{*}b^{*}b^e$	$48*b^{*}b^{*}b^e$	$78*b^{*}b^{*}b^e$	$48*b^{*}b^{*}b^e$	$-28*a^{*}b^{*}b^{*}b^e$	$-36*b^{*}b^{*}b^e$	$-36*b^{*}b^{*}b^e$
$77*a^{*}b^e$	$-78*b^{*}b^{*}b^e$	$-468*b^e$	$-468*b^e$	$175*a^{*}b^e$	$132*b^{*}b^{*}b^e$	$162*b^e$	$-77*a^{*}b^e$	$78*b^{*}b^{*}b^e$	$468*b^e$	$78*b^{*}b^{*}b^e$	$-175*a^{*}b^e$	$-132*b^{*}b^{*}b^e$	$-132*b^{*}b^{*}b^e$
0	$-28*a^{*}b^{*}b^{*}b^e$	$-175*a^{*}b^e$	$-175*a^{*}b^e$	0	$42*a^{*}b^{*}b^{*}b^e$	$77*a^{*}b^e$	$-28*a^{*}b^{*}b^{*}b^e$	$28*a^{*}b^{*}b^{*}b^e$	$175*a^{*}b^e$	$28*a^{*}b^{*}b^{*}b^e$	$-56*a^{*}b^{*}b^{*}b^e$	$-42*a^{*}b^{*}b^{*}b^e$	$-42*a^{*}b^{*}b^{*}b^e$
$-28*a^{*}b^{*}b^{*}b^e$	$36*b^{*}b^{*}b^e$	$132*b^{*}b^{*}b^e$	$132*b^{*}b^{*}b^e$	$-42*a^{*}b^{*}b^{*}b^e$	$-48*b^{*}b^{*}b^e$	$-78*b^{*}b^{*}b^e$	$28*a^{*}b^{*}b^{*}b^e$	$-36*b^{*}b^{*}b^e$	$-132*b^{*}b^{*}b^e$	$-36*b^{*}b^{*}b^e$	$42*a^{*}b^{*}b^{*}b^e$	$48*b^{*}b^{*}b^e$	$48*b^{*}b^{*}b^e$
$-175*a^{*}b^e$	$-132*b^{*}b^{*}b^e$	$-162*b^e$	$-162*b^e$	$-77*a^{*}b^e$	$78*b^{*}b^{*}b^e$	$468*b^e$	$175*a^{*}b^e$	$132*b^{*}b^{*}b^e$	$162*b^e$	$132*b^{*}b^{*}b^e$	$77*a^{*}b^e$	$-78*b^{*}b^{*}b^e$	$-78*b^{*}b^{*}b^e$
$56*a^{*}b^{*}b^{*}b^e$	$42*a^{*}b^{*}b^{*}b^e$	$77*a^{*}b^e$	$77*a^{*}b^e$	$28*a^{*}b^{*}b^{*}b^e$	$-28*a^{*}b^{*}b^{*}b^e$	$-175*a^{*}b^e$	0	$-42*a^{*}b^{*}b^{*}b^e$	$-77*a^{*}b^e$	$-42*a^{*}b^{*}b^{*}b^e$	0	$28*a^{*}b^{*}b^{*}b^e$	$28*a^{*}b^{*}b^{*}b^e$
$-42*a^{*}b^{*}b^{*}b^e$	$-48*b^{*}b^{*}b^e$	$-78*b^{*}b^{*}b^e$	$-78*b^{*}b^{*}b^e$	$-28*a^{*}b^{*}b^{*}b^e$	$36*b^{*}b^{*}b^e$	$132*b^{*}b^{*}b^e$	$42*a^{*}b^{*}b^{*}b^e$	$48*b^{*}b^{*}b^e$	$78*b^{*}b^{*}b^e$	$48*b^{*}b^{*}b^e$	$28*a^{*}b^{*}b^{*}b^e$	$-36*b^{*}b^{*}b^e$	$-36*b^{*}b^{*}b^e$
$-77*a^{*}b^e$	$-78*b^{*}b^{*}b^e$	$-468*b^e$	$-468*b^e$	$-175*a^{*}b^e$	$132*b^{*}b^{*}b^e$	$162*b^e$	$77*a^{*}b^e$	$78*b^{*}b^{*}b^e$	$468*b^e$	$78*b^{*}b^{*}b^e$	$175*a^{*}b^e$	$-132*b^{*}b^{*}b^e$	$-132*b^{*}b^{*}b^e$
$28*a^{*}b^{*}b^{*}b^e$	$28*a^{*}b^{*}b^{*}b^e$	$175*a^{*}b^e$	$175*a^{*}b^e$	$56*a^{*}b^{*}b^{*}b^e$	$-42*a^{*}b^{*}b^{*}b^e$	$-77*a^{*}b^e$	0	$-28*a^{*}b^{*}b^{*}b^e$	$-175*a^{*}b^e$	$-28*a^{*}b^{*}b^{*}b^e$	0	$42*a^{*}b^{*}b^{*}b^e$	$42*a^{*}b^{*}b^{*}b^e$
$28*a^{*}b^{*}b^{*}b^e$	$36*b^{*}b^{*}b^e$	$132*b^{*}b^{*}b^e$	$132*b^{*}b^{*}b^e$	$42*a^{*}b^{*}b^{*}b^e$	$-48*b^{*}b^{*}b^e$	$-78*b^{*}b^{*}b^e$	$-28*a^{*}b^{*}b^{*}b^e$	$-36*b^{*}b^{*}b^e$	$-132*b^{*}b^{*}b^e$	$-36*b^{*}b^{*}b^e$	$-42*a^{*}b^{*}b^{*}b^e$	$48*b^{*}b^{*}b^e$	$48*b^{*}b^{*}b^e$

.....(A.4)

$$[K_{\theta}] = (1/1260) \times (L \sin(\theta)) \times$$

-468*a ^e	-132*a ^{e^2}	175*a ^{e*b^e}	468*a ^e	132*a ^{e^2}	-175*a ^{e*b^e}	-162*a ^e	78*a ^{e^2}	77*a ^{e*b^e}	162*a ^e	-78*a ^{e^2}	-77*a ^{e*b^e}
-132*a ^{e^2}	-48*a ^{e^3}	42*a ^{e^2*b^e}	132*a ^{e^2}	48*a ^{e^3}	-42*a ^{e^2*b^e}	-78*a ^{e^2}	36*a ^{e^3}	28*a ^{e^2*b^e}	78*a ^{e^2}	-36*a ^{e^3}	-28*a ^{e^2*b^e}
-175*a ^{e*b^e}	-42*a ^{e^2*b^e}	0	175*a ^{e*b^e}	42*a ^{e^2*b^e}	-56*a ^{e*b^e}	-77*a ^{e*b^e}	28*a ^{e^2*b^e}	0	77*a ^{e*b^e}	-28*a ^{e^2*b^e}	-28*a ^{e*b^e}
-468*a ^e	-132*a ^{e^2}	-175*a ^{e*b^e}	468*a ^e	132*a ^{e^2}	175*a ^{e*b^e}	-162*a ^e	78*a ^{e^2}	-77*a ^{e*b^e}	162*a ^e	-78*a ^{e^2}	77*a ^{e*b^e}
-132*a ^{e^2}	-48*a ^{e^3}	-42*a ^{e^2*b^e}	132*a ^{e^2}	48*a ^{e^3}	42*a ^{e^2*b^e}	-78*a ^{e^2}	36*a ^{e^3}	-28*a ^{e^2*b^e}	78*a ^{e^2}	-36*a ^{e^3}	28*a ^{e^2*b^e}
175*a ^{e*b^e}	42*a ^{e^2*b^e}	56*a ^{e*b^e}	-175*a ^{e*b^e}	-42*a ^{e^2*b^e}	0	77*a ^{e*b^e}	-28*a ^{e^2*b^e}	28*a ^{e^2*b^e}	-77*a ^{e*b^e}	28*a ^{e^2*b^e}	0
-162*a ^e	-78*a ^{e^2}	77*a ^{e*b^e}	162*a ^e	78*a ^{e^2}	-77*a ^{e*b^e}	-468*a ^e	132*a ^{e^2}	175*a ^{e*b^e}	468*a ^e	-132*a ^{e^2}	-175*a ^{e*b^e}
78*a ^{e^2}	36*a ^{e^3}	-28*a ^{e^2*b^e}	-78*a ^{e^2}	-36*a ^{e^3}	28*a ^{e^2*b^e}	132*a ^{e^2}	-48*a ^{e^3}	-42*a ^{e^2*b^e}	-132*a ^{e^2}	48*a ^{e^3}	42*a ^{e^2*b^e}
-77*a ^{e*b^e}	-28*a ^{e^2*b^e}	0	77*a ^{e*b^e}	28*a ^{e^2*b^e}	-28*a ^{e*b^e}	-175*a ^{e*b^e}	42*a ^{e^2*b^e}	0	175*a ^{e*b^e}	-42*a ^{e^2*b^e}	-56*a ^{e*b^e}
-162*a ^e	-78*a ^{e^2}	-77*a ^{e*b^e}	162*a ^e	78*a ^{e^2}	77*a ^{e*b^e}	-468*a ^e	132*a ^{e^2}	-175*a ^{e*b^e}	468*a ^e	-132*a ^{e^2}	175*a ^{e*b^e}
78*a ^{e^2}	36*a ^{e^3}	28*a ^{e^2*b^e}	-78*a ^{e^2}	-36*a ^{e^3}	-28*a ^{e^2*b^e}	132*a ^{e^2}	-48*a ^{e^3}	42*a ^{e^2*b^e}	-132*a ^{e^2}	48*a ^{e^3}	-42*a ^{e^2*b^e}
77*a ^{e*b^e}	28*a ^{e^2*b^e}	28*a ^{e*b^e}	-77*a ^{e*b^e}	-28*a ^{e^2*b^e}	0	175*a ^{e*b^e}	-42*a ^{e^2*b^e}	56*a ^{e*b^e}	-175*a ^{e*b^e}	42*a ^{e^2*b^e}	0

.....(A.5)

The consistent mass matrix $[M^e]$ of equation (1.28) is given as

$$[M] = (1/3150) \times (\rho h a^e b^e) \times$$

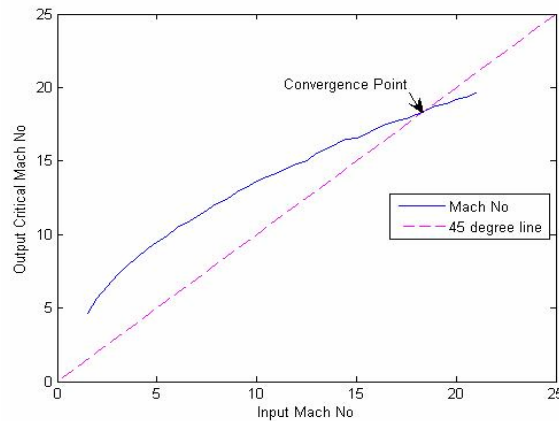
1727	461*a ^e	461*b ^e	613	199*a ^e	-274*b ^e	613	-274*a ^e	199*b ^e	197	-116*a ^e	-116*b ^e
461*a ^e	160*a ^{e^2}	126*b*c*a ^e	199*a ^e	80*a ^{e^2}	-84*b*c*a ^e	274*a ^e	-120*a ^{e^2}	84*b*c*a ^e	116*a ^e	-60*a ^{e^2}	-56*b*c*a ^e
461*b ^e	126*b*c*a ^e	160*b ^{e^2}	274*b ^e	84*b*c*a ^e	-120*b ^{e^2}	199*b ^e	-84*b*c*a ^e	80*b ^{e^2}	116*b ^e	-56*b*c*a ^e	-60*b ^{e^2}
613	199*a ^e	274*b ^e	1727	461*a ^e	-461*b ^e	197	-116*a ^e	116*b ^e	613	-274*a ^e	-199*b ^e
199*a ^e	80*a ^{e^2}	84*b*c*a ^e	461*a ^e	160*a ^{e^2}	-126*b*c*a ^e	116*a ^e	-60*a ^{e^2}	56*b*c*a ^e	274*a ^e	-120*a ^{e^2}	-84*b*c*a ^e
-274*b ^e	-84*b*c*a ^e	-120*b ^{e^2}	-461*b ^e	-126*b*c*a ^e	160*b ^{e^2}	-116*b ^e	56*b*c*a ^e	-60*b ^{e^2}	-199*b ^e	84*b*c*a ^e	80*b ^{e^2}
613	274*a ^e	199*b ^e	197	116*a ^e	-116*b ^e	1727	-461*a ^e	461*b ^e	613	-199*a ^e	-274*b ^e
-274*a ^e	-120*a ^{e^2}	-84*b*c*a ^e	-116*a ^e	-60*a ^{e^2}	56*b*c*a ^e	-461*a ^e	160*a ^{e^2}	-126*b*c*a ^e	-199*a ^e	80*a ^{e^2}	84*b*c*a ^e
199*b ^e	84*b*c*a ^e	80*b ^{e^2}	116*b ^e	56*b*c*a ^e	-60*b ^{e^2}	461*b ^e	-126*b*c*a ^e	160*b ^{e^2}	274*b ^e	-84*b*c*a ^e	-120*b ^{e^2}
197	116*a ^e	116*b ^e	613	274*a ^e	-199*b ^e	613	-199*a ^e	274*b ^e	1727	-461*a ^e	-461*b ^e
-116*a ^e	-60*a ^{e^2}	-56*b*c*a ^e	-274*a ^e	-120*a ^{e^2}	84*b*c*a ^e	-199*a ^e	80*a ^{e^2}	-84*b*c*a ^e	-461*a ^e	160*a ^{e^2}	126*b*c*a ^e
-116*b ^e	-56*b*c*a ^e	-60*b ^{e^2}	-199*b ^e	-84*b*c*a ^e	80*b ^{e^2}	-274*b ^e	84*b*c*a ^e	-120*b ^{e^2}	-461*b ^e	126*b*c*a ^e	160*b ^{e^2}

.....(A.6)

APPENDIX B

Method of Convergence of Critical Mach number

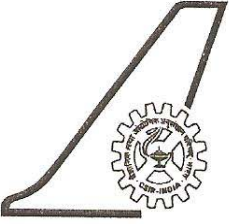

The critical Mach number corresponding to the critical velocity determined by NASTRAN does not match input Mach number, then this input Mach number needs to be updated to this critical velocity. This iterative process is continued by updating the input Mach number till the output and input Mach numbers agree. The converged NASTRAN results so obtained can then be compared with those from the analytical solutions. The convergence study for a panel of aspect ratio $(a/b) = 1$ has been presented in the above table.



Input Mach No.	Output Mach No.
1.5	4.63
2.0	5.70
2.5	6.50
3.0	7.24
3.5	7.85
4.0	8.45
4.5	9.00
5.0	9.50
5.5	9.92
6.0	10.51
6.5	10.80
7.0	11.25
7.5	11.69
8.0	12.10
8.5	12.42
9.0	12.87
9.5	13.16
10.0	13.60
10.5	13.90

Input Mach No.	Output Mach No.
11.0	14.18
11.5	14.50
12.0	14.78
12.5	15.00
13.0	15.50
13.5	15.80
14.0	16.20
14.5	16.50
15.0	16.54
15.5	16.83
16.0	17.20
16.5	17.50
17.0	17.72
17.5	17.86
18.0	18.16
18.5	18.45
19.0	18.75
19.5	18.90
20.0	19.18

DOCUMENTATION SHEET

	NATIONAL AEROSPACE LABORATORIES	Class : Restricted No. of Copies : 15						
Title : Finite Element Studies on Supersonic Panel Flutter under High Thermal Environment with Arbitrary Flow Direction								
Author / s : Somenath Mukherjee, M Manjuprasad, Avinash R , Deepa Sakravarthini S								
Project Co-ordinator : Dr. S Sridhara Murthy								
Division : Structures	NAL Project No. : S -0- 249							
Document No. : TM-ST-0701	Date of Issue : October 2007							
Contents	49	Pages	55	Figures	17	Tables	20	References
External Participation : -								
Sponsor : VSSC (ISRO)								
Approval : Head, Structures Division								
								
Remarks :								
Keywords : Supersonic Panel Flutter, Critical Dynamic Pressure, Flutter Speed, High Thermal Profile, Aspect Ratio, Flow Direction, In-plane Loads.								
Abstract: <p>Panels of re-entry vehicles are subjected to a wide range of flow conditions during ascent and re-entry phases. The flow can vary from subsonic continuum flow to hypersonic rarefied flow with wide ranging dynamic pressure and associated aerodynamic heating. One of the main design considerations is the assurance of safety against panel flutter under the flow conditions characterized by harsh thermal environment. The objectives of this work are to understand the physical principles behind panel flutter under supersonic flow and to make an estimate of the lowering of the critical dynamic pressure (flutter boundary) of the panels due to thermal distributions.</p> <p>Analytical and Finite element formulation have been developed for supersonic flutter analysis of rectangular panels subjected various thermal profiles. The piston theory is used for aerodynamic pressure computations. Panels with simply supported edges (with and without in-plane edge constraints) have been studied.</p> <p>The results obtained by NASTRAN for flow along panel edges are in good agreement with those obtained using the analytical method and the in-house FEM code. From the analysis of the results for various flow directions it has been observed that the flow along the longer sides of the panels is most critical. For simply supported panels with no in-plane edge constraints a thermal gradient can cause a drastic fall in the flutter boundary due to in-plane thermal stresses that effectively reduce structural stiffness. In-plane edge constraints to thermal expansion further lower the flutter boundary.</p> <p>The present study will be useful for the purpose of panel design in re-entry launch vehicles and supersonic fighter aircrafts.</p>								